INSTITUT DE PHYSIQUE DE L'UNIVERSITÉ DE NEUCHATEL

DÉFAUTS TOPOLOGIQUES ET TRANSITIONS DE PHASE D'UN RÉSEAU DE VORTEX SUPRACONDUCTEURS

Thèse présentée à la faculté des Sciences de l'Université de Neuchâtel pour l'obtention du grade de docteur ès Sciences

par

RACINE Georges-André
Physicien diplômé

octobre 1989

IMPRIMATUR POUR LA THÈSE

Défauts topologiques et transitions de phase d'un réseau de vortex supraconducteurs

de M *onsieur Georges-André Racine*

UNIVERSITÉ DE NEUCHATEL

FACULTÉ DES SCIENCES

La Faculté des sciences de l'Université de Neuchâtel, sur le rapport des membres du jury,

MM. les professeurs P. Martinoli, H. Beck et J.L. Olsen (EPF-Zurich)

autorise l'impression de la présente thèse.

Neuchâtel, le *16 octobre 1986*

Le doyen:

François Sigrist

François Sigrist

Les tirés à part ci-joints représentent l'essentiel de la thèse de doctorat dont le titre et le nom de l'auteur sont repris en page de garde. Le texte complet du manuscrit peut être consulté à la bibliothèque de l'institut de Physique de l'Université

rue A.-L. Breguet 1
CH-2000 Neuchâtel

From: PERCOLATION, LOCALIZATION,
AND SUPERCONDUCTIVITY
Edited by Allen M. Goldman
and Stuart A. Wolf
(Plenum Publishing Corporation, 1984)

STATIC AND DYNAMIC PROPERTIES OF COMMENSURATE AND INCOMMENSURATE PHASES OF A TWO-DIMENSIONAL LATTICE OF SUPERCONDUCTING VORTICES

P. Martinoli, H. Beck, M. Nsabimana and G.A. Racine

Institut de Physique, Université de Neuchâtel
CH - 2000 Neuchâtel, Switzerland

INTRODUCTION

Phase transitions in two-dimensional (2D) systems have received considerable attention recently. In several experiments the 2D crystal under consideration is exposed to the force field created by a periodic substrate. Among other situations this is the case of a 2D lattice of superconducting vortices interacting with a periodic pinning potential. As pointed out by Martinoli and coworkers[1-3] some years ago, thin superconducting films, whose thickness is periodically modulated in one dimension, provide such a system. In this lecture we discuss the static and dynamic behaviour of this model system in which the 2D vortex lattice can be driven through a variety of phases[4,5] simply by changing the conditions of flux-line density and/or temperature. In particular, we show how measurements of the critical currents and of the complex rf impedance of thickness-modulated layers can be used to probe the transition of the 2D vortex lattice from a "locked" commensurate (C) phase in registry with the substrate periodicity to a "floating" incommensurate (I) solid phase exhibiting 2D topological order[6,7] or to a fluid-like phase.

THE PHASE DIAGRAM

The phase diagram of 2D crystals interacting with a periodic force field has been studied by a number of authors[4,5]. It is determined by considering, in addition to phonons, two types of topological excitations: domain walls (also called discommensurations,

kinks, or solitons) which trigger the instability of a C-phase with respect to an I-phase (CI-transition) and dislocations which drive melting of the floating-solid phase (I-phase) into a liquid-like phase through the dislocation unbinding mechanism proposed by Kosterlitz and Thouless[6,7].

Dealing with situations where the periodic substrate is, as in our case, anisotropic, a recent theory by Pokrovsky and Talapov[8] (PT) is particularly relevant for the understanding of our experiments, where the 2D vortex lattice experiences the 1D periodic pinning potential created by the thickness modulation. In the following we review some of the basic concepts and results of the PT-theory. The only important difference between our treatment and the one by PT is that in establishing the CI-phase boundary we use, instead of their renormalization-group technique, an alternative approach based on the more transparent *S*elf-*C*onsistent *H*armonic *A*pproximation (SCHA) obtaining a similar result[9,10]. The modifications of the phase diagram resulting from the presence of thermally excited dislocations, which are not included in the PT-model, are briefly discussed at the end of this section.

The CI-Transition at Zero Temperature

We consider a 2D triangular lattice of superconducting vortices, with lattice parameter a, in static interaction with a 1D harmonic potential of amplitude Δ and wave vector $\vec{q}$ ($q = 2\pi/\lambda_q$). We focus our attention on situations where $\vec{q}$ is very close to one of the vectors, $\vec{g}$, of the reciprocal vortex lattice, the condition $\vec{q} = \vec{g}$ defining a configuration of perfect matching between the (undistorted) lattice and the sinusoidal pinning potential. It is assumed that the flux-line lattice is incompressible and, further, that the pinning is weak when compared to the lattice stiffness, i.e. $\Delta < \mu$, where μ is the shear modulus of the vortex lattice[11]. Under these conditions only long-wavelength shear deformations turn out to be relevant and, as a consequence, the vortex lattice can be treated as an elastic continuum. Then, the energy $\mathcal{E}$ of the system can be written as the sum of an elastic contribution due to the pinning-induced lattice distortions and of a potential energy contribution due to the periodic pinning field :

$$\mathcal{E} = \int \left[\frac{\mu}{2}\left(\frac{\partial u}{\partial y} + \frac{\partial v}{\partial x}\right)^2 + \Delta(1 - \cos q\phi)\right] dx\, dy\,. \qquad (1)$$

In writing this expression we have jumped ahead to the conclusion of PT asserting that, at $T = 0$, the ground state of the system is characterized by a quasi 1D deformation field $\vec{w}$, whose components (u,v) in an $(x\text{-}y)$-reference frame with x pointing in a direction

forming an angle of 45^{o} with $\vec{q}$ are given by :

$$u = \delta y , \qquad v = \delta x - \sqrt{2}\,\phi(x) , \tag{2}$$

where $\delta = 1 - (g/q)$ measures the degree of mismatch. It clearly emerges from these expressions that $\vec{w}$ results from the superposition of two uniform shear deformations (one along x and the other along y) and of a 1D transverse field $\phi(x)$ which, for an incompressible lattice, is found to propagate along x[3,8]. In an (x'-y')-coordinate system rotated by 45^{o} with respect to (x-y) the uniform part of $\vec{w}$ is an area conserving deformation consisting of a uniform compression ($\delta > 0$) or expansion ($\delta < 0$) - $\delta x'$ along x' (parallel to $\vec{q}$) combined with a uniform expansion ($\delta > 0$) or compression ($\delta < 0$) $\delta y'$ along y'. This uniform deformation is such that the potential energy contribution to $\mathcal{E}$ vanishes : the vortices are forced to lie at the bottom of the potential wells of the cosine-potential.

To determine $\phi(x)$, we simply minimize the functional $\mathcal{E}[\phi(x)]$ with respect to $\phi(x)$, thereby obtaining the following sine-Gordon equation[12] for the "phase" field $\Phi(x) = q\phi(x)$:

$$\sin\Phi - \ell^2 \frac{\partial^2\Phi}{\partial x^2} = 0 , \tag{3}$$

where $\ell^2 = 2\mu/\Delta q^2$. Its solution in terms of elliptic functions

$$\Phi(x) = \pi + 2\mathrm{am}(x/k\ell) \tag{4}$$

is a stair-shaped function representing a regular sequence of kinks, whose period L is related to k by

$$L = 2k\ell K(k) , \tag{5}$$

where K(k) is a complete elliptic integral of the first kind. Using Eqs. (4) and (5), $\mathcal{E}$ can be expressed as a function of the variational parameter k. Then, minimization of $\mathcal{E}(k)$ with respect to k leads to :

$$|\delta| = (2/\pi)(\Delta/\mu)^{1/2}[E(k)/k] , \tag{6}$$

where E(k) is a complete elliptic integral of the second kind. There are solutions of Eq. (6) satisfying the condition $0 \leq k \leq 1$ only if $|\delta|$ is larger than a critical mismatch δ_c given by :

$$\delta_c = (2/\pi)(\Delta/\mu)^{1/2} \tag{7}$$

For $|\delta| > \delta_c$ $\Phi(x)$ is of the form (4). As a consequence, for $|\delta| > \delta_c$ the vortex lattice is characterized by the formation of a

superstructure, of period L, consisting in a regular 1D sequence of domain walls propagating at 45° with respect to $\vec{q}$. This is the incommensurate I-phase shown in Fig. 1. In constructing this figure we have assumed that the starting matching configuration is that defined by $\vec{q} = \vec{g}_{10}$, $\vec{g}_{10}$ being one of the six nearest-neighbour reciprocal lattice vectors ($g_{10} = 4\pi/a\sqrt{3}$). Since $\delta > 0$, large portions of the lattice shown in Fig. 1 appear to be uniformly compressed along x' and expanded along y' and are essentially commensurate to the underlying 1D periodic substrate. These regions are separated from each other by discommensurations where the phase field $\Phi(x)$, which is essentially constant in the nearly commensurate regions between successive kinks, changes by 2π over distances of the order of $\sim k\ell$. The period L of the superstructure diverges logarithmically as $|\delta|$ approaches δ_c [$k \to 1$ in Eq. (5)].

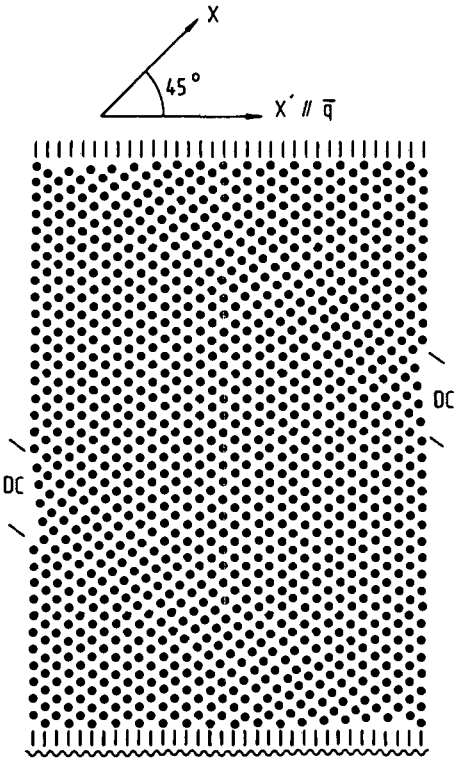

Fig. 1. Incommensurate I-phase for $\delta = 0.13$ ($B/B_{10} = 0.76$). Discommensurations (DC) form a periodic 1D sequence propagating along the x-direction.

For $|\delta| < \delta_c$ there are no solutions of Eq. (6) and, consequently, $\Phi(x)$ is no longer given by Eq. (4). In this case $\mathcal{E}$ has its minimum value when the potential energy contribution due to the periodic pinning field vanishes in Eq. (1), i.e. when $\Phi(x) = 0$ everywhere. This, of course, corresponds to the commensurate C-phase shown schematically in Fig. 2 for $\delta = 0$ (matching configuration $\vec{q} = \vec{g}_{10}$) and for vortex densities corresponding to deviations from perfect registry but still such that $|\delta| < \delta_c$.

The areal free energy density $F_\square$ of the 2D vortex lattice can be written in the form :

$$F_\square = 2\mu\delta^2 - 2\Delta\{[\delta/\delta_c E(k)]^2 - 1\}\,\theta(|\delta| - \delta_c)\,, \qquad (8)$$

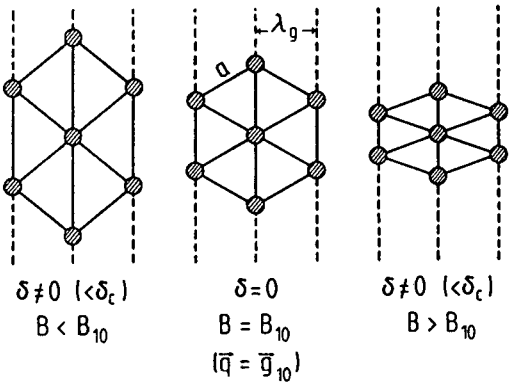

Fig. 2. The fundamental commensurate C_{10}-phase in three different states of deformation.

where $\theta(z)$ is the Heaviside step-function. The first term on the right-hand side of Eq. (8) is the elastic energy density associated with the uniform deformation appearing in both the C- and the I-phase, whereas the second one is due to the phase field $\Phi(x)$ and therefore contributes to $F_\square$ only in the I-phase.

Phase Transitions at Finite Temperatures

To study the CI-transition at finite temperatures, we first consider the case of perfect matching ($\delta = 0$), which is particularly simple. For $\vec{q} = \vec{g}$ the vortices execute a Brownian motion around the equilibrium positions they would assume at the bottom of the potential wells at $T = 0$. Accordingly, the Langevin equation of motion for a vortex at the lattice site $\underline{l}$ can be written as :

$$\eta \dot{\vec{u}}_{\underline{l}} = - \sum_{\underline{l}'}{}' \tilde{G}(\underline{l} - \underline{l}')\vec{u}_{\underline{l}'} - \vec{q}\Delta' \sin(\vec{q} \cdot \vec{u}_{\underline{l}}) + \vec{f}_{\underline{l}}(t) , \qquad (9)$$

where the four terms represent, successively, the viscous damping force, the lattice restoring force, the sinusoidal pinning force and the fluctuating Langevin force acting on the vortex at $\underline{l}$. $\eta^{-1} = R_{\square}/B\phi_0$, where $R_{\square}$ is the sheet flux-flow resistance of the superconducting film, is the mobility[13] of a free vortex, $\tilde{G}(\underline{l} - \underline{l}')$ the elastic matrix and Δ' is related to Δ by $\Delta = n_{\square}\Delta'$, where $n_{\square} = B/\phi_0$ is the areal vortex density. $\vec{f}_{\underline{l}}(t)$ is assumed to have a white noise spectrum defined by the correlation function :

$$\langle f_{\underline{l}\alpha}(t) f_{\underline{l}'\beta}(t') \rangle = 2\eta k_B T \delta_{\alpha\beta} \delta_{\underline{l}\underline{l}'} \delta(t - t') , \qquad (10)$$

stating that the Langevin force is uncorrelated in direction, space and time. To find the mean square fluctuation $\langle u^2 \rangle$ of the vortices, which is the quantity of interest here, it is convenient to expand $\vec{u}_{\underline{l}}(t)$ in normal modes of the vortex lattice[10]. Then, linearizing Eq. (9) within the framework of SCHA and considering, as before, only transverse (t) modes of the lattice the following expression for the t-component of the normal mode amplitude $\vec{u}_{\underline{k}}(\omega)$ is obtained :

$$u_{\underline{k}t}(\omega) = \frac{n_{\square} f_{\underline{k}t}(\omega)}{D_{\underline{k}t} + \Delta_R (\vec{q} \cdot \hat{e}_{\underline{k}t})^2 - i\eta\omega} , \qquad (11)$$

where $D_{\underline{k}t}$ is the matrix element of the (diagonal) dynamical matrix associated with t-modes, $\hat{e}_{\underline{k}t}$ the polarization vector for t-deformations and $f_{\underline{k}t}(\omega)$ the t-Fourier component of the Langevin force. In our SCHA-approach the effective strength, Δ_R, of the pinning field experienced by the vortices is given by :

$$\Delta_R = \Delta \, e^{-\frac{1}{2} q^2 \langle u_{tx}^2 \rangle} , \qquad (12)$$

where $\langle u_{tx}^2 \rangle$ is the mean square t-fluctuation along the x-direction parallel to $\vec{q}$. Therefore, in our treatment the renormalization

effect of the thermal fluctuations, which provides the essential mechanism for the phase transition, enters through a Debye-Waller factor which weakens the periodic pinning force acting on the vortices. To calculate the mean square t-fluctuation $\langle u_t^2 \rangle$ we assume a Debye model, for which $D_{\underline{k}t} = \mu k^2$, and replace the required sum over $\underline{k}$ by an integral over a smooth density of states. Then, in the weak pinning limit $\Delta << \mu$ considered here we deduce from Eqs. (10) and (11) :

$$\langle u_t^2 \rangle = \frac{k_B T}{4\pi\mu} \ln(\mu/\Delta_R) . \tag{13}$$

This result shows quite clearly that in a C-phase the vortex lattice is a 2D solid with conventional long-range order as long as Δ_R remains finite. As expected for 2D systems, $\langle u_t^2 \rangle$ diverges logarithmically as Δ_R vanishes. Since, by equipartition, $\langle u_{tx}^2 \rangle \simeq (1/2)\langle u_t^2 \rangle$ in the limit $\Delta << \mu$, from Eqs. (12) and (13) one deduces :

$$\Delta_R/\Delta = (\Delta/\mu)^{T/(T_{LU} - T)} , \tag{14}$$

where T_{LU} is implicitly given by :

$$k_B T_{LU} = (4/\pi)\mu(T_{LU})\lambda_g^2 . \tag{15}$$

It clearly emerges from Eq. (14) that at the "*L*ocking-*U*nlocking" temperature T_{LU} the vortex lattice undergoes a transition from a perfectly matched ($\delta = 0$) "locked" C-phase ($\Delta_R \neq 0$) to an "unlocked" phase ($\Delta_R = 0$) whose precise nature (floating solid or liquid) will be discussed in a moment. It should be noticed that the expression for T_{LU} deduced with our SCHA-scheme is the same as that obtained by PT using a renormalization-group technique.

For a moderately dense lattice of vortices in dirty superconducting films μ can be written in the form[11] :

$$\mu(T) = (1/2) n_\square (\phi_o/4\pi)^2 \Lambda^{-1}(T) , \tag{16}$$

where $\Lambda = 2\lambda^2/d$ is the effective penetration depth for 2D superconducting layers[10,14]. Since μ is a function of $n_\square = B/\phi_o$, Eq. (15) shows that T_{LU} depends upon the matching configuration under consideration. For a triangular lattice such configurations are defined by[3] :

$$B_{mn} = (\sqrt{3}/2)(\phi_o/\lambda_g^2)(m^2 + n^2 + mn)^{-1} , \tag{17}$$

where m and n are integers. Expressing $\Lambda(T)$ in terms of the normal state sheet resistance $R_{n\square}$ of the film, the transition temperature T_{LU} for the fundamental C_{10}-phase (m = 1, n = 0 corresponding to $\vec{q} = \vec{g}_{10}$) deduced from Eqs. (15) and (16) can be written in the form :

$$T_{LU}/T_c \approx 1 - 0.31(R_{n\square}/R_u) \quad \text{for} \quad R_{n\square} << R_u , \tag{18}$$

where T_c is the BCS-transition temperature and R_u the universal sheet resistance $\hbar/e^2$. LU-transition temperatures for C_{mn}-phases defined by higher values of m and n lie below that given by Eq. (18).

The case of finite mismatch ($\delta \neq 0$) is more delicate. It is clear, however, that, as a consequence of the fluctuating Brownian motion of the vortices, the critical degree of mismatch $\delta_c(T)$ tolerated by a C-phase becomes smaller and smaller as the temperature rises and finally vanishes at $T = T_{LU}$. PT determined the phase boundary $\delta_c(T)$ using a renormalization-group technique, in which the only renormalizable parameter is the pinning potential amplitude Δ[8]. More recently, Puga et al.[15,16] have generalized the PT-treatment by considering the effect of renormalization also on μ and δ. Although several aspects of the CI-phase transition emerging from their calculation turn out to be different from those following from the much simpler SCHA-scheme, the shape of the phase boundary $\delta_c(T)$ resulting from their approach is very similar to that predicted by SCHA. In the latter approximation $\delta_c(T)$ simply follows from Eq. (7) by replacing Δ with its renormalized value Δ_R given by Eq. (14). The resulting phase diagram is shown in Fig. 3, where, instead of $\delta_c(T)$, we have plotted the related quantity $B_c(T) = B_{mn}[1 \pm \delta_c(T)]^2$. Temperatures are conveniently measured in units of T_M, the melting temperature of the 2D vortex lattice[17,18], which, as shown by Eq. (16) and the following equation, is independent of B at moderate vortex densities :

$$k_B T_M = (1/4\pi)\mu(T_M)a^2 . \tag{19}$$

So far, only domain wall excitations, which drive the CI-phase transition, have been included in our analysis. To obtain the complete phase diagram, however, several authors[7,10,19-25] have emphasized that it is necessary to add the effect of thermally excited dislocation pairs[6,7] in order to assess the stability of the I-phase against melting into a fluid-like phase. Recently, Haldane et al.[26] have given a rather unified description of the phase diagram showing that it strongly depends on the order of commensurability p, which for our triangular lattice is related to m and n by $p = (2/\sqrt{3})(m^2 + n^2 + mn)^{1/2}$. For $p < \sqrt{8}$ they find that,

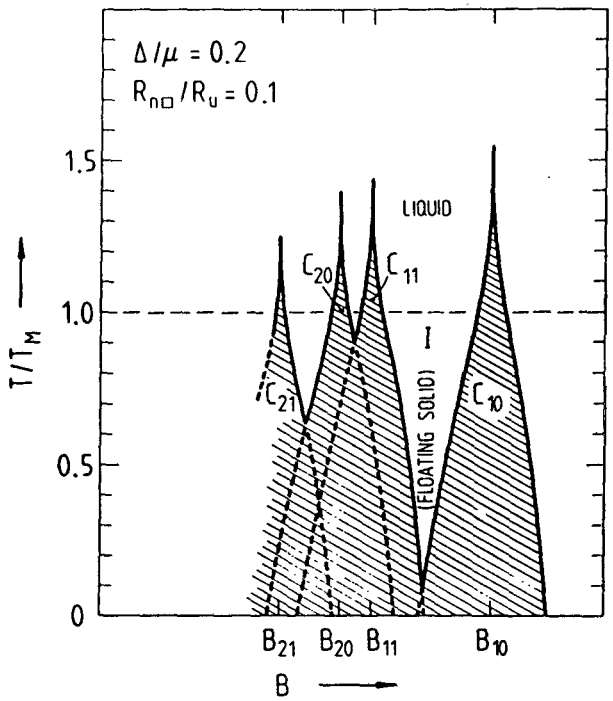

Fig. 3. Phase diagram in the (B,T)-plane of a 2D vortex lattice in a 1D periodic potential.

at finite temperatures, there is always a liquid phase separating the C-phase from the I-phase, whereas for $p > \sqrt{8}$ a direct CI-phase transition is always possible. Although important for a deeper understanding of the physics of 2D system, these features play only a marginal role in the analysis of the experiments reported later on in this lecture. Thus, for simplicity, in constructing the phase diagram of Fig. 3 we have assumed that, in the I-phase, the vortex lattice is a 2D floating solid undergoing a melting transition driven by the unbinding of dislocation dipoles at $T = T_M$. It follows that, if the CI-transition occurs for $T > T_M$, it is actually a transition from a C-phase to a fluid-like phase. This is the case for the lower order C-phases of Fig. 3, where T_{LU} is larger than T_M. A straightforward calculation based on Eqs. (15), (17) and (19) shows, however, that there is a particular commensurate phase, the C_{22}-phase corresponding to $p = 4$, for which T_{LU} becomes equal to T_M. For C-phases of higher order ($p > 4$) T_{LU} is always lower than T_M

and, consequently, a floating solid phase always separates the C-phase from the liquid phase. This agrees with the findings of other authors[19,20,22,23,26].

CRITICAL CURRENTS

To test some of the theoretical ideas put forward in the previous section, critical current (I_c) measurements were performed on thickness modulated granular Al-films as a function of magnetic field and temperature. A combined holographic-photolithographic technique[1] was used to fabricate grating-like film profiles with $\lambda_g \leq 1$ μm and with a relative thickness modulation, $\Delta d/d$, less than 20 - 25%. The most relevant superconducting and normal state parameters of the two Al-films studied in this work are summarized in Table 1.

Since a registered C-phase is pinned by the periodic film structure, a finite current, flowing parallel to the 1D grooves, is required to depin the vortex lattice and, subsequently, to sustain vortex motion in the dissipative flux-flow régime. An I-phase, on the other hand, is not pinned by the periodic substrate, its energy being independent of the relative position of the discommensurations with respect to the pinning potential. Therefore, the critical current for entering the flux-flow régime vanishes in this case.

In Fig. 4 $I_c(B)$-curves for the film Al*1* are shown for different reduced temperatures $t = T/T_c$. Using Eq. (17), one can easily verify that the peak at $B \approx 28$ Gauss corresponds to the fundamental C_{10}-configuration ($p = 2/\sqrt{3}$) shown in Fig. 2, while the small structure at $B \approx 7$ Gauss can be assigned to the C_{11}- and C_{20}-phases which, on account of their strong overlap (see Fig. 3), are hard to resolve from each other. The shape of the $I_c(B)$-peak associated with a given C-phase has been calculated by Burkov and Pokrovsky[27]. In

Table 1. Parameters of the Al-Films

Film	d[Å]	$\Delta d/d$[a]	λ_g[μm]	$R_{n\square}$[Ω]	T_c[K]	$(\xi_0 l)^{1/2}$[Å][b]	$\lambda_L(0)\left(\frac{\xi_0}{l}\right)^{1/2}$[Å][b]
Al1	200	~0.2	0.79	15	1.89	365	4300
Al2	200	~0.2	0.77	35	2.16	223	6140

a Determined by combined optical and electrical methods.
b Calculated using $\rho l = 4 \times 10^{-12}\,\Omega\,\mathrm{cm}^2$ and $\lambda_L(0) = 157$ Å for Al. ξ_0 was scaled from the bulk Al value (1,6 μm) according to our T_c.

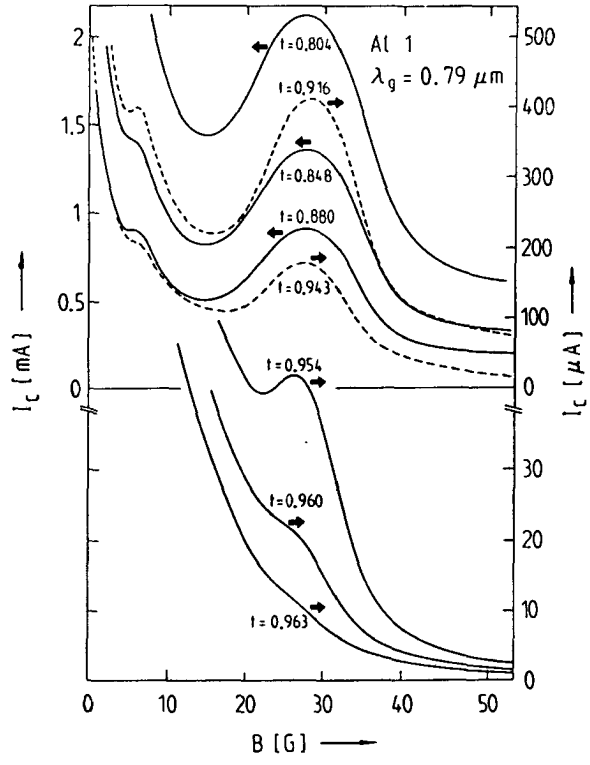

Fig. 4. Critical current vs. magnetic field curves of a thickness modulated film (Al1) at different reduced temperatures $t = T/T_c$.

a sample of finite size it is determined by the stability of the C-phase against the nucleation of a domain wall at the boundary of the film. Therefore, a detailed comparison of the shape of the main peak in Fig. 4 with the theoretical prediction of this model could, in principle, allow a determination of the $C_{10}I$-phase boundary. For two reasons, however, this appears to be, in practice, a difficult problem. The first and more important one is that in our films Δ is found to be of the order of μ, typically $\Delta/\mu \approx 0.9$. Under this condition one expects considerable overlap of the C_{10}-phase with the C_{11}-phase (in Fig. 3 the overlap of the various C-phases is enhanced as Δ/μ increases). This is certainly at the origin of the relatively high shoulder on the low field side of the fundamental I_c-peak in Fig. 4. The second reason is that in real films one is

dealing with unavoidable pinning effects due to randomly distributed inhomogeneities, which result in a finite contribution to I_c even in the I-phase. Clearly, both overlapping and random pinning effects render the analysis of the peak shape quite difficult. We shall therefore concentrate on a much more accessible experimental quantity : the temperature dependent strength $I_{cM}(T)$ of a critical current peak.

For perfect matching the equilibrium position of a vortex is determined[3,28,29] by balancing the Lorentz driving force $\vec{F}_L = d\phi_o(\vec{j} \times \hat{z})$ against the pinning force experienced by the vortex in the effective cosine-potential $\Delta_R'(1 - \cos q\phi)$. This results in the following expression for the transport current density :

$$j = (q\Delta_R'/\phi_o d)\sin\Phi \, . \tag{20}$$

The critical current density, j_{cM}, is reached for $\Phi = \pi/2$, a condition corresponding to vortices located halfway between the bottom and the top of the potential wells. Thus, using Eq. (14) j_{cM} can be written as :

$$j_{cM} = (q\Delta'/\phi_o d)(\Delta/\mu)^{T/(T_{LU} - T)} \, . \tag{21}$$

In order to compare our I_c-data with Eq. (21) we need a model for $\Delta = n_\square \Delta'$, the characteristic energy scale of the pinning mechanism operating in our thickness modulated films. In the thin film limit ($d << \lambda$) the potential energy $\varepsilon(\vec{r})$ of a vortex located at $\vec{r}$ can be expressed by the convolution[30] :

$$\varepsilon(\vec{r}) = \int f(\vec{r}' - \vec{r})\, d(\vec{r}')\, d^2r' \, , \tag{22}$$

where $d(\vec{r}') = d + \Delta d \cos qx$ is the periodically varying film thickness and $f(\vec{r}' - \vec{r})$ the free energy density distribution within the flux line. Using Clem's model[31] for $f(\vec{r}' - \vec{r})$, $\varepsilon(x)$ can be easily evaluated[10] from Eq. (22) in the limits $q\xi < 1$ (ξ is the GL-coherence length) and $q\Lambda >> 1$ of interest here. From the expression for $\varepsilon(x)$ one immediately identifies Δ as :

$$\Delta \approx 2n_\square(\Delta d/d)(\phi_o/4\pi)^2 \Lambda^{-1}(T) \, . \tag{23}$$

This result shows that Δ has the same temperature dependence as μ (Eq. 16), a considerable simplification in the analysis of the I_c-data. By combining Eqs. (21) and (23), I_{cM} can finally be written in the form :

$$\frac{I_{cM}(T)}{I_{cM}(0)} = \frac{\Lambda(0)}{\Lambda(T)} \left(\frac{\Delta}{\mu}\right)^{T/(T_{LU}-T)} , \qquad (24)$$

where $\Delta/\mu \approx 4(\Delta d/d)$. This expression shows very clearly how, with rising temperature, thermal fluctuations further reduce $I_{cM}(T)$ with respect to the BCS-value which corresponds to the limit $T_{LU} \to \infty$. After substraction of the background due to random pinning, which was deduced from a flat but otherwise identical reference film, the critical currents $I_{cM}(T)$ of Al*1* and Al*2* were fitted to Eq. (24) using $I_{cM}(0)$, Δ/μ and T_{LU}/T_c as fitting parameters. The result of this analysis is shown in Fig. 5 where, for comparison, theoretical curves calculated by neglecting the effect of thermal fluctuations are also shown. Good agreement with Eq. (24) is found for a reasonable choice of the parameters. T_{LU}/T_c scales with $R_{n\square}$

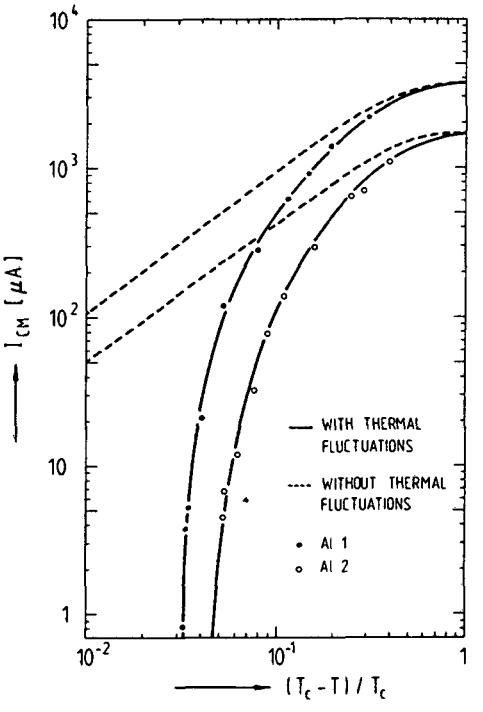

Fig. 5. Temperature dependence of the critical currents of thickness-modulated films in the perfectly registered ($\delta = 0$) C_{10}-phase. The experimental data are fitted to Eq. (24) using : $\Delta/\mu = 0.95$, $T_{LU}/T_c = 0.978$ for Al1 and $\Delta/\mu = 0.90$, $T_{LU}/T_c = 0.972$ for Al2.

approximately as predicted by Eq. (18) where, however, the numerical coefficient 0.31 is found to be about an order of magnitude too small to account for values deduced from the fit of Fig. 5. As for Δ/μ, there is good agreement between the values obtained from the fit and those estimated with $\Delta/\mu \simeq 4(\Delta d/d)$ using the experimental data of $\Delta d/d$ listed in Table 1.

DYNAMICS

The motion of superconducting vortices in a periodic field shows interesting quantum features reminiscent of ac-Josephson phenomena in arrays of superconducting weak links. When the dc driving current I_{dc} exceeds I_c, a particular flux-flow régime characterizes a C-phase. Dynamic coupling of the vortex lattice with the periodic substrate results, in this case, in a highly coherent velocity oscillation of the vortices which, in turn, generates a weak but detectable macroscopic voltage oscillation[2,3], typically in the radiofrequency (rf) range. Indirect evidence for the collective oscillation of the vortices in a C-phase is obtained by exposing thickness-modulated films to rf-radiation. Pinning-induced coupling at rf-frequencies between the oscillating motion of the vortex lattice and the rf-field gives rise to quantum interference transitions in the I-V-curves at discrete values, $E_n = n\nu\lambda_g B$, of the flux-flow dc electric field E_{dc}[3,9,32] ($\nu = \Omega/2\pi$ is the frequency of the rf-radiation). Derivatives of the I-V-characteristics for Al1 exposed to 100 MHz-radiation are shown in Fig. 6. As in the critical current case (Fig. 4), from the evolution of the n = 1 interference transition with increasing temperature one is led to the conclusion that dynamic coupling of the matched vortex lattice to the periodic substrate is totally absent for $T > T_{LU} \simeq 1.85$ K. This provides additional evidence for the occurrence of the locking-unlocking phase transition discussed in the previous section. More detailed information about the dynamics of the 2D vortex lattice in the various phases it can assume on the periodic substrate can be obtained from a study of the complex rf-impedance of thickness-modulated layers. In the rest of this lecture we shall therefore focus our attention on some theoretical and experimental aspects of the dynamic response of the vortex medium to a small oscillating driving field.

Low Temperature Vortex Mobility

At low temperatures ($T << T_{LU}$) thermal fluctuations of the vortices can be neglected. Assuming a driving Lorentz force of the form $\vec{F}_L = d\phi_0(\vec{j}_{rf} \times \hat{z})\exp(-i\Omega t)$, the equation of motion for the position $\vec{r}_l$ of the vortex associated with the lattice site l can

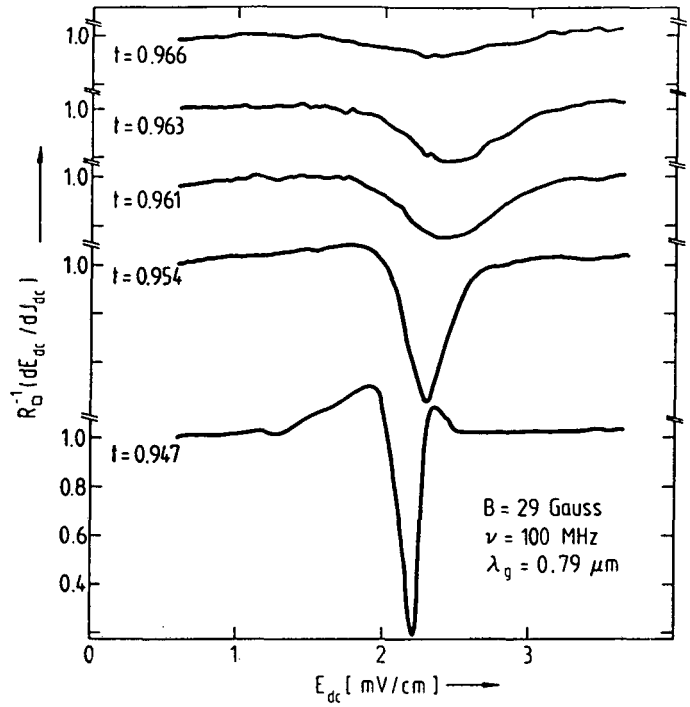

Fig. 6. Derivatives of the rf-excited current-voltage characteristics of Al1 showing the temperature dependence of the n = 1 interference transition.

then be written as[3] :

$$\eta \dot{\vec{r}}_{\underline{l}} = \vec{F}_L + \Delta' \vec{q} \sin \vec{q} \cdot (\vec{r}_{\underline{l}} - \vec{r}_o) - \sum_{\underline{l}'}{}' \frac{\partial W_{\underline{l}\underline{l}'}}{\partial r_{\underline{l}\underline{l}'}} \hat{r}_{\underline{l}\underline{l}'} , \qquad (25)$$

where $W_{\underline{l}\underline{l}'}$ is the interaction energy between the two vortices at $\vec{r}_{\underline{l}}$ and $\vec{r}_{\underline{l}'}$, $r_{\underline{l}\underline{l}'} = |\vec{r}_{\underline{l}} - \vec{r}_{\underline{l}'}|$ and $\vec{r}_o$ defines the relative position of the vortex lattice with respect to the 1D thickness modulation. Thus, the last term in Eq. (25) is the restoring force set up by the lattice in response to the periodic pinning force. To determine the linear response of the vortex medium to $\vec{F}_L$, one should study the oscillating motion of the vortices about their static equilibrium configuration characterized by the deformation field $\vec{w} = (u,v)$ described by Eq. (2). In the continuum limit this problem can be

solved exactly in terms of elliptic functions[33]. To avoid the rather complex algebra of this treatment, in this lecture we shall rely on a simpler perturbative approach which contains, however, all the essential physical features of the vortex dynamics. We assume that Δ is small and, consequently, write the solution of Eq. (25) in the form[3] :

$$\vec{r}_{\underline{l}} = \vec{\underline{l}} + i(\vec{v}_{rf}/\Omega)\, e^{-i\Omega t} + \vec{u}_{\underline{l}} \,, \tag{26}$$

where $\vec{v}_{rf} = (d\phi_o/\eta)(\vec{j}_{rf} \times \hat{z})$. The first two terms in Eq. (26) represent the solution of Eq. (25) in the flat-film case ($\Delta = 0$), whereas $\vec{u}_{\underline{l}}$ is the (small) additional dynamic displacement caused by the (weak) periodic pinning force. Substituting $\vec{r}_{\underline{l}}$, as given by Eq. (26), into Eq. (25) and expanding up to first order in the small quantities $\vec{q} \cdot \vec{u}_{\underline{l}} << 1$ and $(\vec{q} \cdot \vec{v}_{rf})/\Omega << 1$ one obtains :

$$\eta \dot{\vec{u}}_{\underline{l}} = - \sum_{\underline{l}'}{}' \tilde{G}(\underline{l} - \underline{l}')\vec{u}_{\underline{l}'} +$$

$$+ \frac{\Delta'}{2i} \sum_{\vec{q}} \vec{q}(1 + i\vec{q} \cdot \vec{u}_{\underline{l}})\left(1 - \frac{\vec{q} \cdot \vec{v}_{rf}}{\Omega} e^{-i\Omega t}\right) e^{i\vec{q} \cdot (\vec{\underline{l}} - \vec{r}_o)} \,, \tag{27}$$

where the sum in the last term is over $\vec{q}$ and $-\vec{q}$ (two terms). To solve Eq. (27) it is again convenient to expand $\vec{u}_{\underline{l}}$ in (transverse) normal modes of the lattice. The resulting expression contains terms proportional to the normal mode amplitudes $\vec{u}_t(\vec{k},\omega)$, $\vec{u}_t(\vec{k} \pm \vec{q},\omega)$ and $\vec{u}_t(\vec{k} \pm \vec{q}, \omega \pm \Omega)$. Since we are interested in situations where $\vec{q}$ is close to one of the reciprocal lattice vectors $\vec{g}$ ($\vec{q} \approx \vec{g}$), one can set $\vec{u}_t(\vec{k} \pm \vec{q},\omega) \approx \vec{u}_t(\vec{k},\omega)$. Moreover, one can neglect, to a first approximation, terms involving $\vec{u}_t(\vec{k} \pm \vec{q}, \omega \pm \Omega)$ which, arising from the product $(\vec{q} \cdot \vec{u}_{\underline{l}})(\vec{q} \cdot \vec{v}_{rf})/\Omega$ in Eq. (27), are small compared to those proportional to $\vec{u}_t(\vec{k},\omega)$. Then, the equation of motion can be solved for $\vec{u}_t(\vec{k},\omega)$ and the resulting expression is used to calculate the contributions, proportional to $\vec{u}_t(\vec{k} \pm \vec{q}, \omega \pm \Omega)$, neglected in the first order approximation. Finally, a new solution, now accurate to second order in Δ, is worked out from which the vortex velocity $\vec{v}_{\underline{l}}(t) = \dot{\vec{r}}_{\underline{l}}$ is easily deduced. At this point, in order to describe the anisotropic dynamic response of the 2D vortex lattice in the 1D periodic potential, we introduce a vortex mobility tensor $\tilde{\mu}(\Omega)$ defined by $\vec{v}(\Omega) = \tilde{\mu}(\Omega)\vec{F}_L(\Omega)$, where $\vec{v}(\Omega)$ is the vector amplitude of the oscillating flux-flow velocity of the vortex medium. $\vec{v}(\Omega)$ follows by averaging $\vec{v}_{\underline{l}}(t)$ over all vortices of the lattice. An alternative way to describe the lattice response is in terms of a vortex impedance tensor $\tilde{Z}_{v\square}(\Omega)$ defined by $\vec{E}(\Omega) = \tilde{Z}_{v\square}(\Omega)\vec{J}(\Omega)$, where $\vec{E}(\Omega) = -\vec{v}(\Omega) \times \vec{B}$ and $\vec{J}(\Omega) = d\vec{j}(\Omega)$ are, respectively, the electric

field and sheet ($\square$) current amplitudes. Since in a coordinate system with the x-axis pointing in the $\vec{q}$-direction both $\tilde{\mu}(\Omega)$ and $\tilde{Z}_{v\square}(\Omega)$ are found to be diagonal, their components are simply related to each other by $Z_{v\square xx} = n_\square \phi_o^2 \mu_{yy}$ and $Z_{v\square yy} = n_\square \phi_o^2 \mu_{xx}$. Within our perturbative approach we find $\mu_{yy} = \eta^{-1}$, as expected, and :

$$\mu_{xx} = \eta^{-1}\left(1 - \frac{1}{2}\frac{1}{1-i\Omega\tau}\,\delta_{\vec{q},\vec{g}} - \frac{1}{2}\frac{\Delta/\mu}{(1-i\Omega\tau)\left[(b-1)^2 + (\Delta/\mu)\right]}\right) \quad (28)$$

where $b = B/B_{mn}$ and $\tau = \eta/\Delta' q^2$ is the characteristic time for vortex relaxation in the potential wells. In writing the last term of Eq. (28) we have expressed the restoring force constant μk^2, where $\vec{k} = \vec{q} - \vec{g}$ is the wave vector of the pinning-induced shear deformation propagating at 45° with respect to $\vec{q}$, in terms of b (or, alternatively, of δ) using the results of Ref. 3. Real and imaginary parts of μ_{xx} (or $Z_{v\square yy}$), as deduced from Eq. (28), are shown in Fig. 7 (dashed curves) as a function of b. There is a discontinuous jump in both components at $b = 1$ ($\delta = 0$). This reflects the onset of the CI-phase transition which, in our approximation, occurs for $\delta_c = 0$. In the exact calculation[33] both $\mathrm{Re}[Z_{v\square}]$ and $\mathrm{Im}[Z_{v\square}]$ are constant within a C-phase and equal to the corresponding values given by Eq.

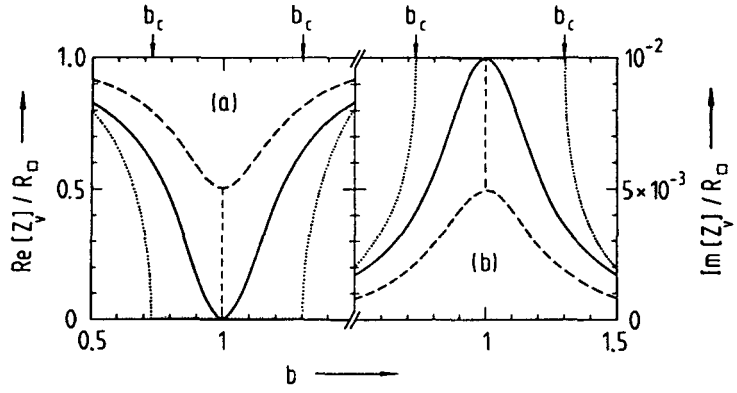

Fig. 7. Real (a) and imaginary (b) part of the normalized vortex impedance as a function of $b = B/B_{mn}$. The driving current flows in the y-direction perpendicular to $\vec{q}$. $\Delta/\mu = 0.05$, $\Omega\tau = 10^{-2}$. The significance of the various curves is explained in the text.

(28) for $b = 1$ ($\vec{q} = \vec{g}$) up to the critical mismatch δ_c (dotted curves in Fig. 7). One way to correct for the jump at $b = 1$ and to improve our approximation is to write μ_{xx} in the following form :

$$\mu_{xx} = \eta^{-1}\left(1 - \frac{\Delta/\mu}{(1 - i\Omega\tau)[(b-1)^2 + \Delta/\mu]}\right) \qquad (29)$$

As shown in Fig. 7 (full curves) this expression provides a reasonable description of the actual lattice response. For this reason we shall rely on Eq. (29) for the interpretation of the sheet conductance measurements reported in the last section of this lecture.

There is a simple physical interpretation for the general behaviour of $\mathrm{Re}[Z_{v\square}]$ and $\mathrm{Im}[Z_{v\square}]$ shown by Fig. 7. In a C-phase dissipation arises from the excitation, in the viscous vortex medium, of a collective mode in which the vortices oscillate in phase around their equilibrium positions at the bottom of the potential wells. In the I-phase additional dissipation results from the excitation of the soliton superstructure. Thus, $\mathrm{Re}[Z_{v\square}]$ must have its minimum value in a C-phase. $\mathrm{Im}[Z_{v\square}]$, on the other hand, measures the delay in lattice response caused by the periodic pinning structure. As the effect of pinning is strongest in a C-phase, $\mathrm{Im}[Z_{v\square}]$ is obviously largest in such a phase.

Sheet Conductance Measurements

To measure the dynamic response of the vortices in our thickness modulated layers, we rely on the two-coil experimental technique developed by Fiory and Hebard[34]. The superconducting film is mounted in a transverse plane between two coaxial closely-spaced coils, one (drive coil) providing the rf-excitation of the vortex medium, the other (receive coil) to detect its rf-response. For an isotropic 2D superconductor, as it is the case for a flat ($\Delta = 0$) superconducting film, Fiory and Hebard have shown that, in the limit of weak screening, the rf-voltage amplitude $V_R(\Omega)$ at the receive coil due solely to the rf-response currents flowing in the sample is proportional to $\Omega^2 G_\square I_D(\Omega)$, where $G_\square = Z_\square^{-1}$ is the (complex) sheet conductance of the film and $I_D(\Omega)$ the (constant) amplitude of the rf-current in the drive coil. A straightforward extension of this calculation to our anisotropic samples shows that, in the same weak-screening limit, $V_R(\Omega)$ can be written in the form :

$$V_R(\Omega) = \Omega^2 I_D(\Omega)(K_1 G_{\square xx} + K_2 G_{\square yy}) , \qquad (30)$$

where K_1 and K_2 are constants depending on the geometry of the

sample and of the two-coil configuration and the x-axis is still pointing in the $\vec{q}$-direction. According to Fiory and Hebard[35 36], $\tilde{z}_{\square} = \tilde{G}_{\square}^{-1}$ can be expressed as a series connection of the vortex impedance $\tilde{z}_{v\square}$ with the kinetic inductance $L_k = (1/2)\mu_0\Lambda$ associated with the superfluid background. Thus, using the results of the previous section, $Z_{\square xx} = G_{\square xx}^{-1} = (n_{\square}\phi_0^2/\eta) + i\Omega L_k$ and $Z_{\square yy} = G_{\square yy}^{-1} = n_{\square}\phi_0^2\mu_{xx} + i\Omega L_k$, where μ_{xx} is given by Eq. (29). Using typical parameters for our Al-films (Table 1), it can be easily verified that, except very close to T_c or at extremely low magnetic fields, the kinetic inductance term is always much smaller than the vortex impedance and can therefore be neglected in the analysis of most of our experimental data. Furthermore, in the vicinity of a registered phase ($B \approx B_{mn}$), the lattice configuration of interest here, $Z_{\square xx} \approx n_{\square}\phi_0^2/\eta$ varies weakly with B, while, on the contrary, $Z_{\square yy} \approx n_{\square}\phi_0^2\mu_{xx}$ shows pronounced structures (Fig. 7). Thus, if one uses a modulation technique, in which B is weakly modulated

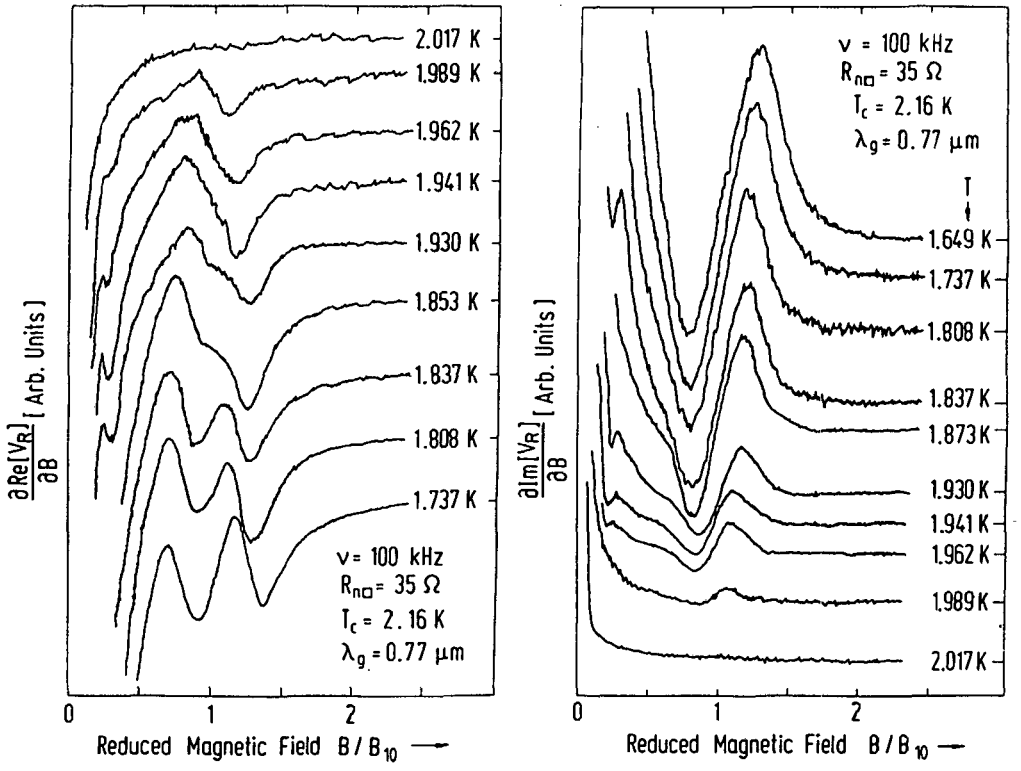

Fig. 8. Derivative curves of the in-phase and out-of phase components of the rf-response of Al2 as a function of B. Marks on the vertical axis denote the zero-level of the signal.

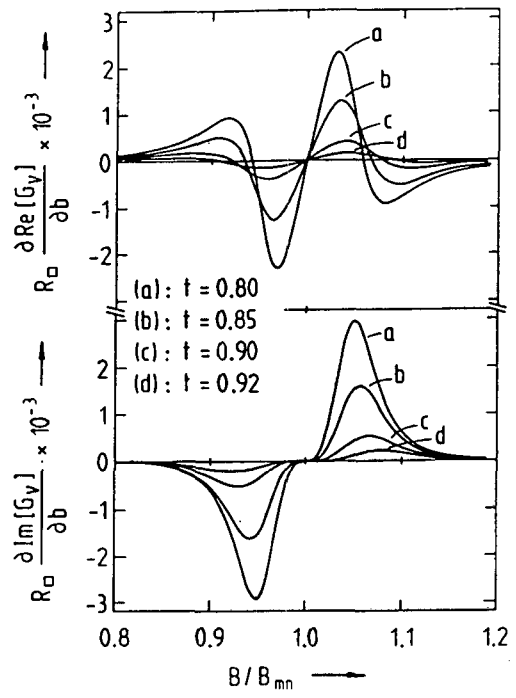

Fig. 9. Theoretical derivative curves of the complex vortex impedance for Al2 as deduced from Eqs. (29) and (14) using $\Delta/\mu = 0.9$. See text for the determination of $\Omega\tau(T)$.

($\delta B \approx 0.1$ Gauss) at a low frequency ($\sim$ 2 Hz), the signal one actually detects at the receive coil will be essentially proportional, for $B \approx B_{mn}$, to $\partial G_{\square yy}/\partial B$. In Fig. 8 sets of curves at different temperatures for the in-phase and out-of-phase components of the 100 kHz-signal for Al2, measured with a conventional phase-sensitive technique, are shown as a function of B. There are pronounced structures in both the real and imaginary parts in the vicinity of $B_{10} \approx 30$ Gauss (weaker structures are visible also in correspondence of the unresolved C_{11}- and C_{20}-phases). The shape of these structures should now be compared with that predicted by Eq. (29). To this purpose, in Fig. 9 we show theoretical curves calculated from Eq. (29) where, in an attempt to partially include the effect of thermal fluctuations, Δ/μ was replaced by Δ_R/μ and $\tau = \eta/\Delta_R' q^2 = \eta/q\phi_o dj_{cM}$ [Eq. (20)] was estimated using the j_{cM}-data for Al2 of Fig. 5. While there is good qualitative agreement for both components of the signal at low temperatures, the evolution of the

structures about B_{10} with rising temperature is quite different from that predicted by Eq. (29). In particular, as one expects from the temperature dependence of the critical mismatch δ_c tolerated by a C-phase, their width becomes narrower and narrower as T approaches T_{LU}, a feature which does not emerge from the theoretical curves of Fig. 9. Clearly, a more elaborated model which takes into account, in particular, diffusion phenomena of "corrugated" domain walls should be worked out in order to describe the dynamic response of the periodically pinned 2D vortex lattice at high temperatures ($T \lesssim T_{LU}$). This, as well as the study of other features of the rf-response (in particular of the origin of the drastic crossover in response at low magnetic fields in Fig. 8) will be the object of future research in our laboratory.

ACKNOWLEDGEMENTS

We would like to thank J.R. Clem, V.L. Pokrovsky and M. Puga for stimulating discussions. This work has been supported by the Swiss National Science Foundation.

REFERENCES

1. O. Daldini, P. Martinoli, J. L. Olsen, and G. Berner, Vortex-line pinning by thickness modulation of superconducting films, Phys. Rev. Lett. 32:218 (1974).
2. P. Martinoli, O. Daldini, C. Leemann, and B. Van den Brandt, Josephson oscillation of a moving vortex lattice, Phys. Rev. Lett. 36:382 (1976).
3. P. Martinoli, Static and dynamic interaction of superconducting vortices with a periodic pinning potential, Phys. Rev. B 17:1175 (1978).
4. P. Bak, Commensurate phases, incommensurate phases and the devil's staircase, Rep. Prog. Phys. 45:587 (1982).
5. J. Villain, Theories of commensurate-incommensurate transitions on surfaces, in: "Ordering in two dimensions", S. K. Sinha, ed., North Holland, Inc., New York (1980).
6. J. M. Kosterlitz, and D. J. Thouless, Ordering, metastability and phase transitions in two-dimensional systems, J. Phys. C 6:1181 (1973).
7. D. R. Nelson, and B. I. Halperin, Dislocation-mediated melting in two dimensions, Phys. Rev. B 19:2457 (1979).
8. V. L. Pokrovsky, and A. L. Talapov, The theory of two-dimensional incommensurate crystals, Zh. Eksp. Teor. Fiz. 78:269 (1980) [Sov. Phys. JETP 51:134 (1980)].

9. P. Martinoli, H. Beck, M. Nsabimana, and G.-A. Racine, Locking-unlocking transition of a two-dimensional lattice of superconducting vortices, Physica 107B:455 (1981).
10. P. Martinoli, M. Nsabimana, G.-A. Racine, H. Beck, and J. R. Clem, Locked and unlocked phases of a two-dimensional lattice of superconducting vortices, Helv. Phys. Acta 55:655 (1982).
11. A. T. Fiory, Measurements of the shear modulus of the superconducting mixed state of thin films, Phys. Rev. B 8:5039 (1973).
12. F. C. Frank, and J. H. van der Merwe, One-dimensional dislocations, Proc. Roy. Soc. (London) A198:205 (1949).
13. J. Bardeen, and M. J. Stephen, Theory of the motion of vortices in superconductors, Phys. Rev. 140A:1197 (1965).
14. M. Tinkham, in: "Introduction to superconductivity", McGraw-Hill, Inc., New York (1975).
15. M. W. Puga, E. Simanek, and H. Beck, Renormalization-group approach to commensurate-incommensurate transitions in two dimensions, Phys. Rev. B 26:2673 (1982).
16. M. W. Puga, E. Simanek, and H. Beck, Commensurate-incommensurate transitions, to appear in Helv. Phys. Acta (1983).
17. B. A. Huberman, and S. Doniach, Melting of two-dimensional vortex lattices, Phys. Rev. Lett. 43:950 (1979).
18. D. S. Fisher, Flux-lattice melting in thin-film superconductors, Phys. Rev. B 22:1190 (1980).
19. J. V. José, L. P. Kadanoff, S. Kirkpatrick, and D. R. Nelson, Renormalization, vortices, and symmetry-breaking perturbations in the two-dimensional planar model, Phys. Rev. B 16:1217 (1977) [Erratum, Phys. Rev. B 17:1477 (1978)].
20. S. Ostlund, Relation between lattice and continuum theories of two-dimensional solids, Phys. Rev. B 23:2235 (1981).
21. S. Ostlund, Incommensurate and commensurate phases in asymmetric clock models, Phys. Rev. B 24:398 (1981).
22. J. Villain, and P. Bak, Two-dimensional Ising model with competing interactions : floating phase, walls and dislocations, J. Physique 42:657 (1981).
23. S. N. Coppersmith, D. S. Fisher, B. I. Halperin, P. A. Lee, and W. F. Brinkman, Dislocations and the commensurate-incommensurate transition in two dimensions, Phys. Rev. Lett. 46:549 (1981).
24. T. Bohr, V. L. Pokrovsky, and A. L. Talapov, Commensurate-incommensurate phase transition in continuous media containing dislocations, Pis'ma Zh. Eksp. Teor. Fiz. 35:165 (1982) [Sov. Phys. JETP Lett. 35:203 (1982)].
25. T. Bohr, Dislocations in the commensurate-incommensurate transition, Phys. Rev. B 25:6981 (1982).

26. F. D. M. Haldane, P. Bak, and T. Bohr, Phase diagramms of surface structures from Bethe-Ansatz solutions of the quantum sine-Gordon model, preprint (1982).
27. S. E. Burkov, and V. L. Pokrovsky, Critical currents and electric fields of two-dimensional systems, J. Low Temp. Phys. 44:423 (1981).
28. P. Martinoli, J. L. Olsen, and J. R. Clem, Superconducting vortices in periodic pinning structures, J. Less-Common Metals 62:315 (1978).
29. P. Martinoli, and J. R. Clem, Pinning in periodic superconducting structures, in: "Inhomogeneous superconductors-1979", D. U. Gubser, T. L. Francavilla, S. A. Wolf, and J. R. Leibowitz, ed., American Institute of Physics, New York (1980).
30. A. Schmid, and W. Hauger, On the theory of vortex motion in an inhomogeneous superconducting film, J. Low Temp. Phys. 11:667 (1973).
31. J. R. Clem, Simple model for the vortex core in a type II superconductor, J. Low Temp. Phys. 18:427 (1975).
32. P. Martinoli, O. Daldini, C. Leemann, and E. Stocker, A. C. quantum interference in superconducting films with periodically modulated thickness, Solid State Comm. 17:205 (1975).
33. V. L. Pokrovsky, private communication.
34. A. T. Fiory, and A. F. Hebard, Radio-frequency complex-impedance measurements on thin film two-dimensional superconductors, in: "Inhomogeneous superconductors-1979", D. V. Gubser, T. L. Francavilla, S. A. Wolf, and J. R. Leibowitz, ed., American Institute of Physics, New York (1980).
35. A. F. Hebard, and A. T. Fiory, Recent experimental results on vortex processes in thin-film superconductors, in: "Ordering in two dimensions", S. K. Sinha, ed., North Holland, Inc., New York (1980).
36. A. F. Hebard, and A. T. Fiory, Vortex dynamics in two-dimensional superconductors, Physica 109 & 110 B:1637 (1982).

LT-17 (Contributed Papers)
U. Eckern, A. Schmid, W. Weber, H. Wühl (eds)

DYNAMICS OF COMMENSURATE AND INCOMMENSURATE PHASES OF A 2D LATTICE OF SUPERCONDUCTING VORTICES

F. PATTHEY, G.-A. RACINE, C. LEEMANN, H. BECK and P. MARTINOLI

Institut de Physique, Université de Neuchâtel, CH - 2000 Neuchâtel, Switzerland

A study of the complex rf vortex response of superconducting films with periodically modulated thickness is presented. Structures emerging at well defined vortex densities in both the real and imaginary parts of the response are shown to arise from a commensurate-incommensurate phase transition of the vortex lattice triggered by solitons.

Modulated structures whose period is incommensurable with that of the underlying lattice have been studied in a variety of condensed-matter systems. In particular, the very existence of commensurate (C) and incommensurate (I) phases has been demonstrated for a 2D lattice of vortices in thin superconducting films whose thickness is periodically modulated in one direction (1). Here we study the anisotropic dynamic response of C and I vortex phases to a small oscillating driving force $\vec{f}$.

At low temperatures the phase diagram of 2D crystals exposed to a periodic 1D force field is determined only by soliton excitations which trigger the CI-transition (1,2). For an incompressible lattice the I-phase is characterized by a 1D soliton superlattice, of period P, varying under 45^0 with respect to $\vec{q}_0$, the wave vector of the thickness modulation. For an infinite 2D vortex crystal at T = 0 the CI-phase transition, where $P \to \infty$, occurs when the deviations from a matching configuration $\vec{q}_0 = \vec{g}_{mn}$ ($\vec{g}_{mn}$ is a reciprocal vortex lattice vector) are such that the mismatch $\delta = 1 - (g_{mn}/q_0)$ reaches $\delta_c = (2/\pi)(\Delta/\mu)^{1/2}$, Δ being the strength of the cosine potential and μ the shear modulus of the vortex lattice.

To study the dynamic response of the pinned vortex medium, we rely on a modified version of the technique devised by Fiory and Hebard (3). With the vortex crystal in a C-phase, this method does not excite transverse modes of an infinite lattice and coupling to shear modes only arises from the finite size of the sample and/or from residual random pinning. In an I-phase the 1D periodic sequence of solitons breaks the translational symmetry of the vortex lattice, thereby allowing intrinsic coupling of the driving field to transverse modes of the soliton superlattice. Thus, structures due to the CI-transition at $\delta = \delta_c$ are expected in the complex vortex impedance of modulated layers as the magnetic field B is swept across B_{mn}, the value defining perfect matching (1).

The experiments were performed on a modulated ($2\pi/q_0$ = 0.73 μm) Al-film (T_c = 2.05 K, d = 500 Å, R_n = 25 Ω). As shown by the insert of Fig. 2, excitation of the vortex lattice was provided by two coils, D_1 and D_2, placed on top of the film and driven in opposition by a 5 μA rf-current I_{rf}. The voltage V due solely to the film response was phase sensitively detected by a receive coil R placed between D_1 and D_2 and lying in a plane perpendicular to the film. Because of the 3 Hz field modulation used to discriminate against vortex motion independent pick-up, the detected signals are proportional to $\partial V/\partial B$. To study the angular dependence of the response, the R-coil was oriented either parallel or orthogonal to D_1 and D_2 and the whole arrangement rigidly rotated with respect to $\vec{q}_0$. We denote by (α,β) a coil configuration such that $\vec{f}$ acts in the the α-direction while the R-coil detects the response arising from the projection of vortex motion along the β-direction.

Data taken at 3 MHz and at different temperatures are shown in Fig. 1 for the (y,y)- configuration. Pronounced structures show up in both components of $\partial V/\partial B$ around B_{10}. These structures gradually disappear at higher temperatures. In Fig. 2 signals corresponding to

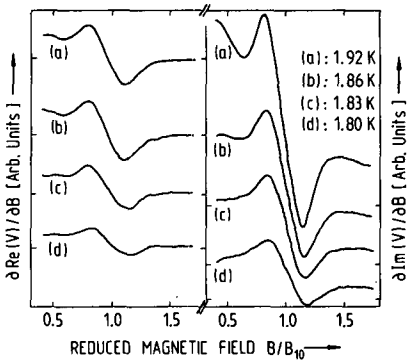

FIG. 1 : Field derivatives of the vortex response at 3 MHz. Coil configuration (y,y).

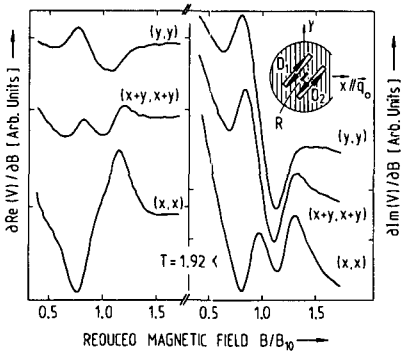

FIG. 2 : Field derivatives of the complex vortex response at 3 MHz for three different coil configurations.

three different coil configurations are shown for T = 1.92 K. A striking feature emerging from these data is the appearance, as the coils are progressively rotated from the (y,y) towards the (x,x)-configuration, of a large new signal which washes out almost completely the structure resulting from the CI-phase transition in $\partial Re(V)/\partial B$ and generates additional structure in $\partial Im(V)/\partial B$. The fact that it does not show up at lower temperatures indicates that it cannot be associated with the type of CI-phase transition described above.

Our calculation of the vortex lattice response has been done in the continuum approximation (1,2). The equation of motion for the displacement field $\vec{w} = \vec{w}_{st} + \vec{u}$ is linearized in the deviation $\vec{u}$ from the static deformation $\vec{w}_{st}$. The finite size L of the sample has been accounted for by allowing for boundary solitons (BS) in a C-phase (4). The I-phase and the C-phase with BS are matched where $P(\delta) = L$. In practice, the appropriate L may be considerably shorter than the actual sample length, approximately of the order of the mean distance between lattice imperfections which interrupt the coherence of the soliton lattice.

The equation of motion of the dissipative (viscosity η) vortex continuum (Lamé coefficients λ,μ) driven by $\vec{f}$ in the periodic potential $U(\phi) = U(w_x + \delta x)$ has the form

$$\eta(\partial\vec{u}/\partial t) = \hat{O}\vec{u} + \vec{f} \quad , \qquad (1)$$

where $\hat{O} = (\lambda + \mu)\nabla\nabla\cdot + \mu\nabla^2 - \hat{q}_0 U''(\phi_{st})\hat{q}_0$.. Its solution $\vec{u}(\vec{r},t)$ can be expressed in terms of the eigenfunctions of the operator $\hat{O}$.

Using London's and Maxwell's equations, the voltage V due exclusively to vortex motion is shown to be given by an integral over Fourier components of the deviation, $\delta\vec{\Phi}$, of the fluxoid field $\vec{\Phi}$ (3,5) from its static value :

$$\delta\vec{\Phi}(\vec{q},t) = \phi_0(\hat{q} \times \hat{z})[\hat{q}\cdot\vec{u}(\vec{q},t)] \quad . \qquad (2)$$

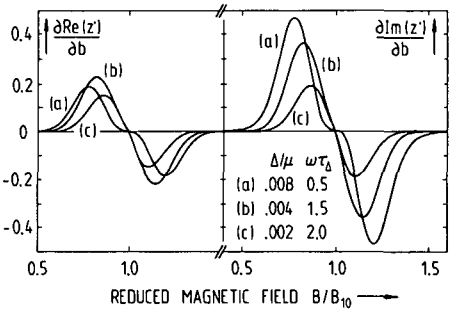

FIG. 3 : Theoretical field derivatives of $z' = Z'/R_f$. $L = 30(2\pi/q_0)$, $b = B/B_{10}$.

Introducing the solution of Eq. (1) into Eq. (2), V can be approximately expressed by $V = GZ'I_{rf}$, where G describes geometry and orientation of D_1, D_2 and R and the impedance $Z'(B,T,\omega)$ contains the vortex dynamics.

For practical calculations we have chosen a piece-wise parabolic potential U. Thus, in the I-phase $U''(\phi_{st})$ yields a Kronig-Penney (KP) potential with distance P between the "spikes". For the C-phase with BS we use periodic boundary conditions, a procedure resulting again in a KP-potential with P replaced by L. The eigenfunctions of $\hat{O}$ are characterized by a Bloch wave vector $\vec{K}$. If the geometry dependent quantities vary slowly, only small $\vec{q}$ are needed in Eq. (2) and the relevant $\vec{K}$ are the reciprocal lattice vectors $\vec{Q}$ corresponding to the periodic potential in $\hat{O}$. For an incompressible lattice ($\lambda \to \infty$) the $\vec{Q} = 0$-mode doesn't contribute to Z'.

Theoretical field derivatives of Z' are shown in Fig. 3. As shown in Ref. 1, rising temperatures can be simulated by decreasing values of Δ/μ and of the relaxation rate $\tau^{-1} = q_0^2\Delta/\eta$. Comparison with the data of Fig. 1 shows good qualitative agreement for the B-dependence as well as for the relative magnitude of the real and imaginary parts of the signal. When T is high enough (1), the structures in Z' around B_{mn} disappear, as observed experimentally. Details of the temperature and angular dependences, however, need further analysis.

REFERENCES

(1) P. Martinoli, M. Nsabimana, G.-A. Racine, H. Beck and J.R. Clem, Helv. Phys. Acta 55 (1982) 655.
(2) V.L. Pokrovsky and A.L. Talapov, Phys. Rev. Lett. 42 (1979) 65.
(3) A.T. Fiory and A.F. Hebard, AIP Conf. Proc. 58 (1980) 293.
(4) S.E. Burkov and V.L. Pokrovsky, J. Low Temp. Phys. 44 (1981) 423.
(5) J. Pearl, Vortex Theory of Superconductive Memories, Thesis (Polytechnic Institute of Brooklyn, New York, 1965).

Helvetica Physica Acta, Vol. 58 (1985) 427–442 0018–0238/85/020427–16$1.50 + 0.20/0

Dynamics of commensurate and incommensurate vortex phases in a two-dimensional superconductor

By P. Martinoli, H. Beck, G. A. Racine, F. Patthey and Ch. Leemann, Institut de Physique, Université de Neuchâtel, CH-2000 Neuchâtel, Switzerland

(19. X. 1984)

In honor of Emanuel Mooser's 60th birthday

Abstract. A study of the complex vortex response at radio-frequencies of superconducting films with periodically modulated thickness is reported. In this system, depending on vortex density and temperature, the two-dimensional vortex lattice undergoes a transition from a commensurate (C) phase in registry with the film periodicity to an incommensurate (I) phase. The CI-transition is triggered by soliton excitations which, at low temperature, form a one-dimensional superlattice in the I-phase. Structures emerging at well defined vortex densities in both the real and imaginary parts of the rf vortex response are interpreted as a signature of the CI-transition. A theoretical calculation of the vortex response based on the dynamics of an elastic dissipative vortex continuum with discommensurations provides a good qualitative description of the rf-signals observed at low temperatures. It is shown that the mechanism responsible for the occurrence of the structures at the CI-transition is the break of translational symmetry caused by the formation of the soliton superlattice.

I. Introduction

Modulated structures whose period is incommensurable with that of the underlying lattice have been discovered and studied in a variety of condensed-matter systems [1]. They are usually observed in systems showing two competing periodicities as, for instance, rare-gas monolayers adsorbed at the surface of a solid, crystals with two interpenetrating incommensurate sublattices, metallic conductors undergoing a Peierls transition leading to the formation of a charge density wave and helical or sinusoidal magnetic structures incommensurable with the crystal lattice in certain rare-earth compounds. Moreover, the very existence of commensurate (C) and incommensurate (I) phases has also been demonstrated for a two-dimensional (2D) lattice of vortices in thin superconducting films whose thickness is periodically modulated in one direction [2–7]. In this paper we show how some of the features characterizing the CI-phase transition of the 2D vortex crystal in modulated layers can be seen in a study of the dynamic response of the vortices to a small rf driving field.

The phase diagram of 2D crystals exposed to a periodic 1D force field has been studied by Pokrovsky and Talapov [8] and by Martinoli et al. [7]. At low temperatures, where melting phenomena driven by the unbinding of thermally excited dislocation pairs [9–11] are expected to be irrelevant, it is determined by considering only one particular type of topological excitations, called solitons (or

discommensurations), which trigger the instability of a C-phase with respect to an I-phase. The I-phase is characterized by a 1D soliton superlattice, of period P, varying, for the incompressible lattice of vortices, under an angle 45° with respect to $\vec{q}_0$, the wave vector of the 1D thickness modulation. For an infinite 2D vortex crystal at $T=0$ a CI-phase transition, at which P diverges, occurs whenever the deviations from a configuration $\vec{q}_0 = \vec{g}_{mn}$ corresponding to perfect matching ($\vec{g}_{mn}$ is a reciprocal vortex lattice vector) are such that the mismatch parameter $\delta = 1-(g_{mn}/q_0)$ reaches the critical value $\delta_c = (2/\pi)(\Delta/\mu)^{1/2}$, where Δ is the amplitude of the cosine pinning potential and μ the shear modulus [12] of the vortex lattice.

To study the dynamic response of the pinned vortex medium, we rely on a modified version of the two-coil technique devised by Fiory and Hebard [13]. With the vortex crystal in a C-phase, this method does not excite transverse modes of an infinite lattice. In such a phase coupling to lattice shear modes only arises from the finite size of the sample, from Umklapp (U)-processes and/or from residual random pinning. In a I-phase, on the other hand, the 1D periodic sequence of solitons breaks the translational symmetry of the vortex lattice, thereby allowing intrinsic coupling of the oscillating driving field to transverse modes of the soliton superlattice. Thus, pronounced structures reflecting the occurrence of the CI-phase transition at $\delta = \delta_c$ are expected in the rf complex vortex response of thickness modulated layers as the transverse magnetic field B (and, consequently, δ) is swept across the value, B_{mn}, defining a configuration of perfect matching ($\delta = 0$) [5, 7]. The detection of these structures (Section II) as well as their theoretical interpretation (Section IV) in terms of a model for the dynamics of the 2D vortex medium in its different phases (Section III) are the central object of the present paper.

II. Experimental results

The experiments were performed on a thickness modulated ($\lambda_0 = 2\pi/q_0 = 0.73\ \mu$m) granular Al-film [2, 7] with a BCS-transition temperature, T_c, of 2.05 K, a normal-state sheet resistance, $R_{n\square}$, of 25 Ω, an average thickness, d, of 500 Å and a relative thickness modulation, $\Delta d/d$, of the order of 10%. As shown in Fig. 1, excitation of the vortex medium was provided by two elongated rectangular (20 mm × 1.8 mm) coils, D_1 and D_2, placed at an average height, h_D, of approximately 0.5 mm above the film surface and driven in opposition by a 5 μA rf-current, I_a, of angular frequency ω. With this coil configuration, the driving 'Meissner' sheet supercurrent density $\vec{J}_M$ flowing in that region of the film, located between D_1 and D_2, which significantly contributes to the rf-voltage detected by the receive coil R (Fig. 1) is nearly unidirectional and parallel to the unit vector $\hat{D}$ shown in Fig. 1. The square-shaped (4 mm × 4 mm) receive coil R lies in a plane perpendicular to the superconducting layer, the distance, h_R, of closest approach of its winding to the film surface being of the order of 0.1 mm. The rf-signal, which was phase-sensitively detected against rf-drive, contains two contributions. The first one, denoted by V, arises from the total sheet current density $\vec{J}$ flowing in the modulated film. $\vec{J}$ is the sum of $\vec{J}_M$ and of the 'vortex' sheet current density $\vec{J}_v$ resulting from the oscillating motion of the vortices driven by $\vec{J}_M$ [14]. The second one is the pick-up signal at R due to the rf-current circulating in D_1 and

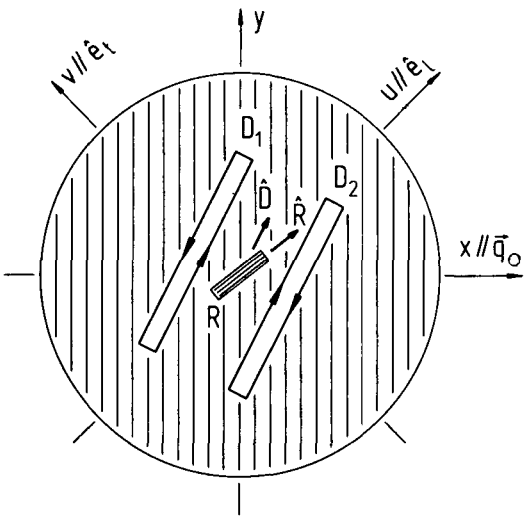

Figure 1
Geometry of the drive (D_1 and D_2)–receive (R) coil configuration used to measure the rf-response of commensurate and incommensurate vortex phases in a thickness-modulated superconducting film.

D_2. In order to discriminate the genuine film response V against the spurious film-independent pick-up, a low-frequency ($\sim$3 Hz) weak-field ($\Delta B \sim 0.1$ gauss) modulation technique was used. As a result, the actually detected signal at R turns out to be proportional to $\partial V/\partial B$. Moreover, to study the angular dependence of the rf-response, the orientation of the R-coil relative to D_1 and D_2, as determined by the unit vectors $\hat{R}$ and $\hat{D}$ in Fig. 1, was changed and the whole coil arrangement was rigidly rotated with respect to $\vec{q}_0$, which is assumed to be parallel to the x-axis. We shall denote by (α, β) a coil configuration such that the driving force on the vortices, $\vec{F}_L = (\phi_0/c)(\vec{J}_M \times \hat{z})$, provided by D_1 and D_2 is in the α-direction while the orientation of the R-coil is such that it detects the response arising from the projection of vortex motion along the β-direction.

Data taken at 3 MHz and at different temperatures are shown in Fig. 2 for the (y, y)-coil configuration. Pronounced structures in both the in-phase and out-of-phase components of $\partial V/\partial B$ emerge from a monotonically varying background around $B_{10} = (\sqrt{3}/2)(\phi_0/\lambda_0^2) = 33.6$ gauss, the field defining the fundamental matching configuration ($m = 1$, $n = 0$) [5–7]. These structures, which are not resolved at low temperatures ($T < 1.7$ K), show up at about 1.7 K and, after an initial growth in strength with increasing temperature, gradually disappear at higher temperatures. It should also be noticed that, although comparable in magnitude, the imaginary part of the signal around B_{10} is systematically larger than its real part. Even though not so well-resolved as those shown in Fig. 2, structures reflecting the CI-phase transition of the 2D vortex lattice were observed also in the vicinity of B_{11} and B_{20}, the fields corresponding to higher-order matching configurations.

Signals corresponding to the (x, x)-coil configuration are shown in Fig. 3. While similar in shape and magnitude to those of the (y, y)-configuration at low temperatures [curve (d)], these structures are quite different from those shown in Fig. 2 at high temperatures [curve (a)]. A striking feature emerging from these

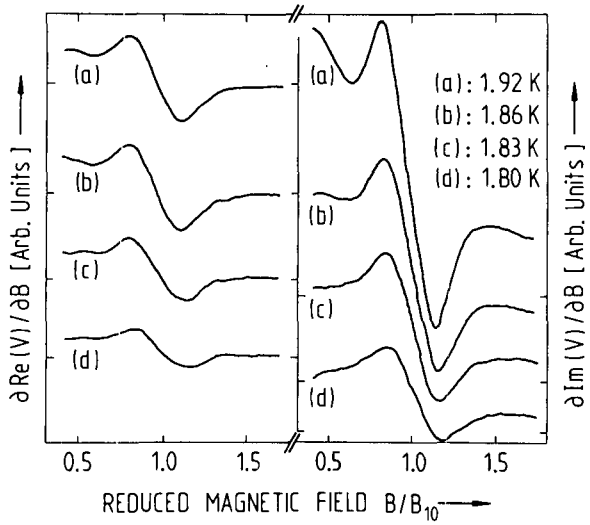

Figure 2
Magnetic field dependence of the complex vortex response of a thickness-modulated Al-film measured at 3 MHz with the (y, y)-coil configuration. Marks on the vertical axis denote the zero-level of the signals.

data is the appearance, as T progressively rises, of a new signal which washes out almost completely the (weak) structure assigned to the low-temperature CI-transition in the real component and generates additional structure in the imaginary part of $\partial V/\partial B$. The strong anisotropic character of the high-temperature signals shows up quite clearly as the coils are progressively rotated form the (y, y)-towards the (x, x)-configuration. While at low temperatures only minor

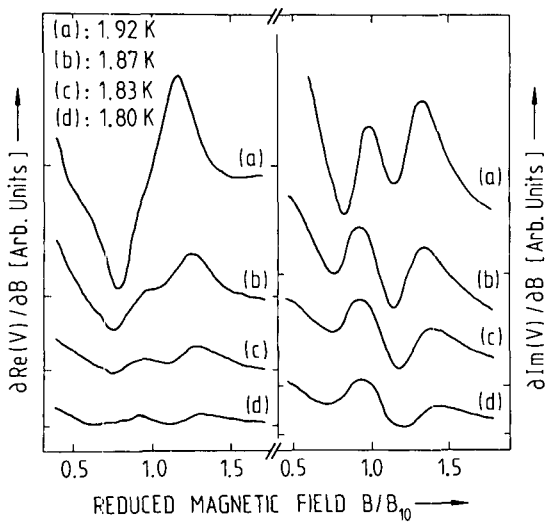

Figure 3
As Fig. 2, but for the (x, x)-coil configuration.

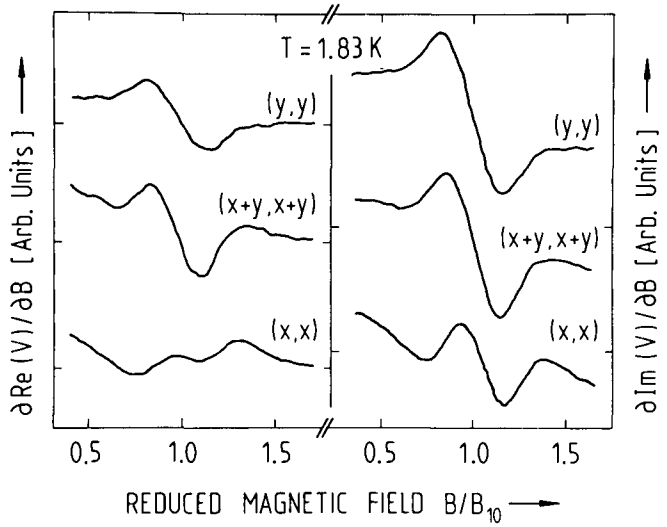

Figure 4
Magnetic field dependence of the low-temperature complex vortex response at 3 MHz for three different coil configurations. The film is the same as in Fig. 2.

changes in the shape of the structures are observed (Fig. 4), profound modifications in the form of both components of $\partial V/\partial B$ occur at higher temperatures (Fig. 5). Although the origin of the additional feature observed when the measuring coils are in the (x, x)-configuration might well be related to the CI-phase transition of the 2D vortex crystal, the fact that it only shows up at high temperatures indicates that it cannot be associated with the type of low-temperature CI-transition described in this paper.

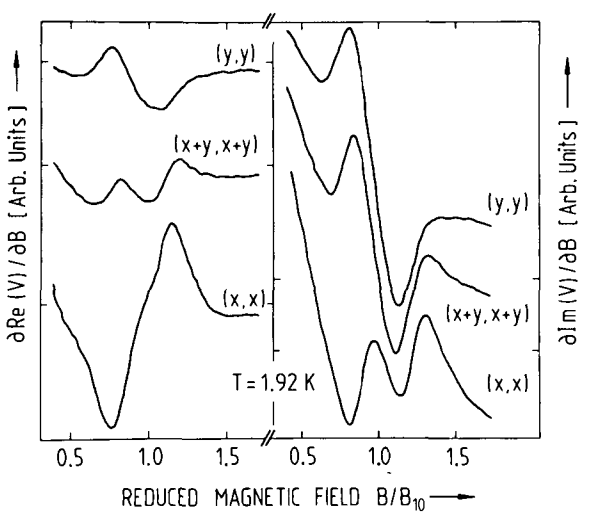

Figure 5
As Fig. 4, but at a higher temperature.

III. Vortex dynamics

To study the dynamics of the vortex lattice in its various phases, we shall focus our attention on situations where $\vec{q}_0$ is close to one of the reciprocal vortex lattice vectors $\vec{g}_{mn}$. Furthermore, it is assumed that the periodic pinning potential is weak when compared to the lattice stiffness, i.e. $\Delta < \mu$. Under this condition the triangular vortex lattice can be treated as an isotropic 2D elastic continuum with Lamé coefficients λ and μ [15]. Then, the equation of motion for the deformation field $\vec{w}$ of the dissipative 2D vortex medium driven by the oscillating force $\vec{F}_L = (B/c)(\vec{J}_M \times \hat{z})$ in the periodic potential $U(\phi)$, where $\phi = w_x + \delta x$ is the displacement of the vortices, in the x-direction (Fig. 1), with respect to the bottom of the corresponding potential wells, can be written in the form [15]:

$$\eta \frac{\partial \vec{w}}{\partial t} = \mu \nabla^2 \vec{w} + (\lambda + \mu) \nabla \nabla \cdot \vec{w} - \nabla_\phi U + \vec{F}_L, \tag{1}$$

where $\eta = B^2/c^2 R_\square$ is the viscosity coefficient [16] expressed in terms of the sheet flux-flow resistance $R_\square$. Since we are interested in the linear dynamic response of the vortex lattice to the driving force $\vec{F}_L$, it is convenient to write $\vec{w}$ in the form $\vec{w} = \vec{w}_e + \vec{s}$ and to expand equation (1) to first order in the deviation $\vec{s}$ from the static (equilibrium) deformation field $\vec{w}_e$. As shown in Ref. 7, for an infinite 2D vortex crystal $\vec{w}_e$ consists in a homogeneous area-conserving deformation in a C-phase onto which a 1D soliton lattice is superposed in an I-phase. In Section III(C) we shall show how the finite size of the sample can be accounted for by allowing for the nucleation of boundary solitons in a C-phase [17]. Linearizing equation (1) in the small dynamic displacement $\vec{s}$ one obtains the following equation for vortex motion:

$$\eta \frac{\partial \vec{s}}{\partial t} + \hat{\mathbb{L}} \vec{s} = \vec{F}_L, \tag{2}$$

where $\hat{\mathbb{L}}$ is a 2×2 matrix operator whose components are given by:

$$\hat{\mathbb{L}}_{\alpha\beta} = -\mu \nabla^2 \delta_{\alpha\beta} - (\lambda + \mu) \nabla_\alpha \nabla_\beta + \hat{q}_{0\alpha} U''(\phi_e) \hat{q}_{0\beta} \tag{3}$$

with $\phi_e = w_{ex} + \delta x$. Equation (2) is a linear inhomogeneous partial differential equation, whose solutions $\vec{s}(\vec{r}, t)$ can be expressed in terms of the normalized eigenvectors $\vec{\Phi}_{\mathbf{K}}$ and of the eigenvalues $E(\vec{K})$ of the operator $\hat{\mathbb{L}}$:

$$\hat{\mathbb{L}} \vec{\Phi}_{\mathbf{K}} = E(\vec{K}) \vec{\Phi}_{\mathbf{K}}. \tag{4}$$

Taking an $e^{i\omega t}$-time dependence for $\vec{F}_L$, the ω-Fourier component, $\vec{s}_\omega(\vec{r})$, of $\vec{s}(\vec{r}, t)$ can be written as:

$$\vec{s}_\omega(\vec{r}) = \sum_{\mathbf{K}} \frac{\langle \Phi_{\mathbf{K}} \mid F_{L\omega} \rangle}{i\eta\omega + E(\vec{K})} \vec{\Phi}_{\mathbf{K}}(\vec{r}), \tag{5}$$

where the scalar product is defined by:

$$\langle f \mid g \rangle = \frac{1}{L^2} \int (\vec{f}^* \cdot \vec{g}) d^2 r, \tag{6}$$

L being the (linear) size of the sample, which is assumed to have a square shape.

At this stage the problem is reduced to that of finding the eigenvectors $\vec{\Phi}_{\mathbf{K}}$ and eigenvalues $E(\vec{K})$ of the operator $\hat{\mathbb{L}}$ in the different phases assumed by the vortex lattice. For the sake of simplicity, in the mathematical calculations it is convenient to choose, instead of a cosine potential, a piece-wise parabolic periodic potential such that $U(\phi_e) = (1/2)\kappa\phi_e^2$ in the interval $-(\lambda_0/2) \leqslant \phi_e \leqslant (\lambda_0/2)$.

A. *The commensurate* (C) *phase* ($\delta < \delta_c$)

In the ground state of an infinite 2D vortex crystal in a C-phase ($\delta < \delta_c$) each vortex of the lattice lies at the bottom of a potential well, i.e. $\phi_e \equiv 0$ everywhere [7]. As a consequence, the curvature $U''(\phi_e)$ of the periodic potential experienced by the vortices, which appears in the last term of equation (3), is a constant which takes the value κ for our particular choice of $U(\phi_e)$. Then, for an incompressible ($\lambda \to \infty$) lattice of vortices the solutions of equation (4) are plane waves of the form:

$$\vec{\Phi}_{\mathbf{K}}(\vec{r}) = \hat{e}_t(\vec{K}) e^{i\vec{K}\cdot\vec{r}}, \tag{7}$$

where $\hat{e}_t(\vec{K})$ is a polarization vector for transverse lattice deformation modes $[\hat{e}_t(\vec{K}) \cdot \vec{K} = 0]$ and the wave vector $\vec{K}$ is confined within the first Brillouin zone. The corresponding eigenvalues are given by:

$$E(\vec{K}) = \mu K^2 + \kappa \frac{K_y^2}{K^2}, \tag{8}$$

where K_y is the component of $\vec{K}$ along the y-direction, perpendicular to $\vec{q}_0$, shown in Fig. 1. As expected, for vortex motion perpendicular to the grooves of the periodic potential, i.e. for shear modes such that $\vec{K} \cdot \vec{q}_0 = 0$, there is a gap, of value κ, in the dispersion relation (8) at $K = 0$.

B. *The incommensurate* (I) *phase* ($\delta > \delta_c$)

The 1D soliton superlattice, which characterizes the ground state of the 2D vortex crystal in the I-phase ($\delta > \delta_c$), is described by the 'phase' field ϕ_e, a stair-shaped function [7] varying only along a direction u which, for the incompressible vortex lattice, is found to form an angle of 45° with the x-axis (Fig. 1). Since ϕ_e only depends on u and is such that $\phi_e(u + nP) = \phi_e(u) + n\lambda_0$, the last term of equation (3), which contains the curvature $U''(\phi_e)$, is a periodic function of u with period $P: U''[\phi_e(u + nP)] = U''[\phi_e(u)]$. Anticipating external forces $\vec{F}_L$ which are almost spatially homogeneous (see Section IV), this suggests to look for solutions of equation (4) varying only along the u-direction, i.e. of the form $\vec{\Phi}_{\mathbf{K}} = \vec{\Phi}_{\mathbf{K}}(u)$. It is then easily seen that, in the $u - v$ reference frame of Fig. 1, equation (4) takes the form of a (1D) matrix Schrödinger equation for the 'spinor' field $\vec{\Phi}_{\mathbf{K}}(u)$ describing the motion of a particle in the 1D periodic potential $U''[\phi_e(u)]$. As a consequence, $\vec{\Phi}_{\mathbf{K}}(u)$ is a Bloch function of the form:

$$\vec{\Phi}_{\mathbf{K}}(u) = \vec{\Psi}_{\mathbf{K}}(u) e^{iKu}, \tag{9}$$

where $\vec{\Psi}_{\mathbf{K}}(u)$ is such that $\vec{\Psi}_{\mathbf{K}}(u + nP) = \vec{\Psi}_{\mathbf{K}}(u)$ and the Bloch wave vector $\vec{K}$ is parallel to the u-direction. To find an explicit form of the eigenfunctions $\vec{\Phi}_{\mathbf{K}}(u)$, we rely on our particular choice for $U(\phi_e)$. In this case the static soliton solution

$\phi_e(u)$, in the limit $\lambda \to \infty$, is given by [18]:

$$\phi_e(u) = \frac{\lambda_0}{2} \sum_n \chi(u - nP) \left[\frac{\sinh \varepsilon(u - nP)}{\sinh(\varepsilon P/2)} + 2n \right], \tag{10}$$

where $\chi(z)$ is such that $\chi(z) = 1$ for $-(P/2) \leq z \leq (P/2)$ and vanishes otherwise and $\varepsilon^2 = \kappa/2\mu$. The period P is related to the mismatch parameter δ and, consequently, to the magnetic field B by [18]:

$$\frac{\delta}{\delta_c} = \coth(\varepsilon P/2) + \frac{(\varepsilon P/2)}{\sinh^2(\varepsilon P/2)}, \tag{11}$$

where $\delta_c = \varepsilon\lambda_0/4\sqrt{2}$. With $\phi_e(u)$ given by equation (10) one can easily show that $U''[\phi_e(u)]$ yields a Kronig-Penney potential of the form:

$$U''[\phi_e(u)] = \kappa - \frac{2\kappa}{\varepsilon} \tanh(\varepsilon P/2) \sum_n \delta(u - nP). \tag{12}$$

Since $U''[\phi_e(u)] = \kappa$ between the (negative) 'spikes' of the periodic potential (12), we look, in these regions, for solutions of the form:

$$\vec{\Phi}_{\mathbf{K}}(u) = \vec{a}_{\mathbf{K}} e^{ik_{\mathbf{K}}u} + \vec{b}_{\mathbf{K}} e^{-ik_{\mathbf{K}}u} \tag{13}$$

which, after substitution in equation (4), lead to the following expression for $E(\vec{K})$:

$$E(\vec{K}) = \tfrac{1}{2}(\kappa + 2\mu k_{\mathbf{K}}^2). \tag{14}$$

Relying on Bloch's theorem, which requires that $\vec{\Phi}_{\mathbf{K}}(u + P) = e^{iKP}\, \vec{\Phi}_{\mathbf{K}}(u)$, one can match at a 'spike' solutions corresponding to successive regions by imposing continuity as in quantum mechanics [19]. For an incompressible lattice this procedure leads to the following condition for $k_{\mathbf{K}}$:

$$\cos KP = \cos(k_{\mathbf{K}} P) - \varepsilon P \tanh(\varepsilon P/2) \frac{\sin(k_{\mathbf{K}} P)}{k_{\mathbf{K}} P}. \tag{15}$$

The dispersion relation $E(\vec{K})$ resulting from equations (14) and (15) is shown in Fig. 6, where the 'acoustical' branch located betwen $-\pi/P$ and $+\pi/P$ corresponds to the so-called phason mode [20] of the soliton lattice.

It will be shown in Section IV that the relevant Bloch wave vectors $\vec{K}$ of our experiments are the non-vanishing reciprocal vectors $\vec{G}$ of the 1D soliton superlattice $[G = n(2\pi/P)]$. In this particular case and for the incompressible vortex lattice $\vec{\Phi}_{\mathbf{G}}(u)$ takes the simple form:

$$\vec{\Phi}_{\mathbf{G}}(u) = A\hat{e}_t(\vec{K}) \cos k_{\mathbf{G}} \left(u - \frac{P}{2} \right), \tag{16}$$

where $\hat{e}_t(\vec{K})$ is a polarization vector for transverse excitation modes of the 1D soliton lattice, i.e. $\hat{e}_t(\vec{K}) \cdot \vec{K} = 0$ with $\vec{K}$ parallel to the u-axis (see Fig. 1), and $k_{\mathbf{G}}$ is one (still unspecified) solution of equation (15) for $\vec{K} = \vec{G}$ (see Section IV for a discussion of this point). The amplitude A is determined by the condition $\langle \Phi_{\mathbf{K}} \mid \Phi_{\mathbf{K}'} \rangle = \delta_{\mathbf{K}\mathbf{K}'}$:

$$A^2 = 2 \left[1 + \frac{\sin(k_{\mathbf{G}} P)}{k_{\mathbf{G}} P} \right]^{-1}. \tag{17}$$

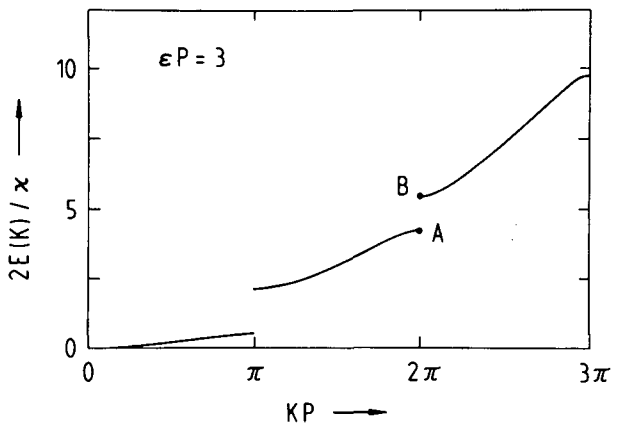

Figure 6
Dispersion relation for the soliton lattice of an incommensurate vortex phase. Only even standing waves, corresponding to points like A, contribute to the vortex response measured in our experiments.

C. *Size effects*

For a sample of finite size one should allow for the nucleation of soliton-like topological excitations at the edges (boundary solitons) when the bulk of the vortex lattice is in a C-phase [17]. The situation is schematically illustrated by Fig. 7, where, for the sake of simplicity, we have assumed that the orientation of our square sample is such that its edges form an angle of ±45° with the x-axis. Then, boundary solitons will form at two opposite edges of the sample. As shown by Fig. 7(a), for $P(\delta) < L$ the vortex lattice is in the I-phase. It is assumed that in this case edge effects have negligible influence on the vortex dynamics, so that the calculations for the infinite incommensurate crystal of Section III(B) still apply as long as $P(\delta) < L$. For $\delta < \delta_0$, where δ_0 is such that $P(\delta_0) = L$, soliton nucleation is possible only at two opposite boundaries of the sample, the bulk of the vortex lattice being in a C-phase. For $\delta = \delta_0$ [Fig. 7(b)], i.e. $P(\delta_0) = L$, one single soliton, having precisely the same features as those studied in the previous subsection, exactly fits into the sample. Thus, its amplitude at the edges, as deduced from equation (10), is $\phi_e(L/2) = -\phi_e(-L/2) = \lambda_0/2$. For $P(\delta) > L$, i.e. $\delta < \delta_0$, the size L is too small for the system to be able to accommodate a 'complete' soliton, i.e. a soliton for which the 'phase' jump $\phi_e(L/2) - \phi_e(-L/2)$ amounts to λ_0. As a consequence, the soliton amplitude at the edges decreases as δ is progressively reduced below δ_0 and finally vanishes for $\delta = 0$ [Fig. 7(c)]. An obvious phenomenological way to take into account this effect is to write the soliton amplitude at the boundaries as $\phi_e(L/2) = -\phi_e(-L/2) = (\lambda_0/2)(\delta/\delta_0)^\gamma$, where the (positive) exponent γ turns out to be equal to 1 if one applies the result of Ref. 17 to our piece-wise parabolic potential. To study the dynamics of superconducting vortices in a C-phase with boundary solitons [$P(\delta) > L$], it is convenient to impose again periodic boundary conditions to equation (4) by requiring that $\tilde{\Phi}_{\mathbf{K}}(u + L) = e^{iKL}\tilde{\Phi}_{\mathbf{K}}(u)$. The problem is then formally identical to that solved in Section III(B), the (fixed) periodicity, however, being now L rather than $P(\delta)$. For our particular choice of $U(\phi_e)$ the above expression for the soliton amplitude at the boundaries

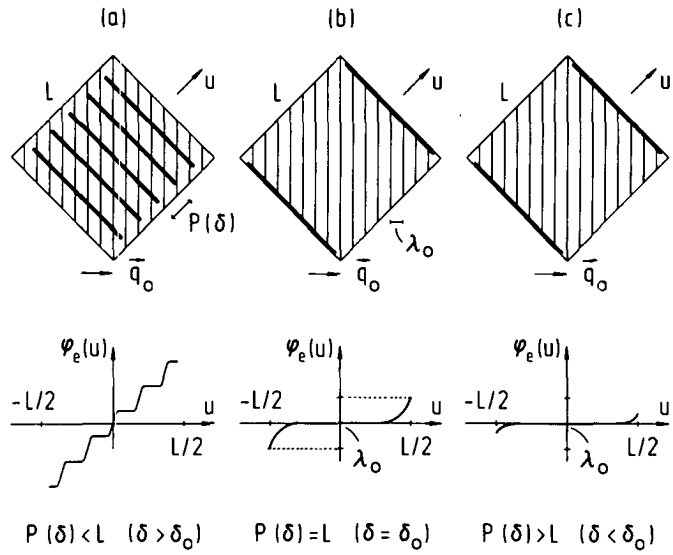

Figure 7
Solitons in a sample of finite size: (a) Incommensurate (striped) phase; (b) Commensurate phase showing boundary solitons with full amplitude at the edges; (c) Commensurate phase with boundary solitons of reduced edge amplitude.

suggests a Kronig-Penney potential of the form (for $\delta < \delta_0$):

$$U''[\phi_e(u)] = \kappa - \frac{2\kappa}{\varepsilon}(\delta/\delta_0)^{\gamma} \tanh(\varepsilon L/2) \sum_n \delta(u - nL). \tag{18}$$

From equation (12), which is valid for $P(\delta) \leq L$ ($\delta \geq \delta_0$), and equation (18), which applies for $P(\delta) \geq L$ ($\delta \leq \delta_0$), it is seen that the I-phase and the C-phase with boundary solitons are correctly matched at $\delta = \delta_0$, where $P(\delta_0) = L$. It is also clear that, with $U''[\phi_e(u)]$ given by equation (18), equations (14)–(17) of the previous subsection still apply when $P(\delta) > L$ with the prescription, however, of replacing P by L everywhere and with an additional factor $(\delta/\delta_0)^{\gamma}$ in the last term of equation (15).

What is the appropriate size L in real films? To answer this nontrivial question, we notice that the granular structure of the modulated Al-films used in our experiments represents a dense system of randomly distributed weak pinning centers acting on the vortices. Under these circumstances long-range positional order no longer exists in the vortex medium. An almost periodic vortex lattice only occurs within domains whose size is determined by the Larkin-Ovchinnikov correlation length R_c [21], which is typically of the order of 10–50 lattice constants [22]. Therefore, we expect the appropriate L for our films to be approximately of the order of R_c and, consequently, much smaller than the actual sample size.

IV. The rf vortex response

Relying on the vortex dynamics studied in the previous Section, we shall now derive a theoretical expression for the rf-signal V generated in the receive coil R

by the sheet current density $\vec{J}(\vec{r}, t) = \vec{J}_M(\vec{r}, t) + \vec{J}_v(\vec{r}, t)$ flowing in a thickness-modulated film in response to the rf-excitation provided by the drive coils D_1 and D_2 (see Section II and Fig. 1).

We consider a very thin superconducting film, such that $d \ll \lambda$, where λ is the temperature dependent penetration depth. Under this condition, the superconducting layer is truly two-dimensional and can be thought of as being confined to a plane which, for convenience, is assumed to be the $z = 0$-plane. The 'usual' current density $\vec{j}(\vec{r}, z, t)$ is then related to the 'sheet' current density $\vec{J}(\vec{r}, t)$ simply by $\vec{j} = \delta(z)\vec{J}$. To calculate the rf-response V, we consider the vector potential variation $\delta\vec{A}(\vec{r}, z, t) = \vec{A}(\vec{r}, z, t) - \vec{A}_a(\vec{r}, z, t)$ due to $\vec{J}(\vec{r}, t)$, $\vec{A}$ and $\vec{A}_a$ being, respectively, the (total) vector potential generated by $\vec{J}$ and $\vec{j}_a$ (the current density associated with the rf-current I_a circulating in D_1 and D_2) and the vector potential created by $\vec{j}_a$ alone. Then, if the driving frequency, $\omega/2\pi$, is not too high, $\vec{A}(\vec{r}, z, t)$ satisfies, in all space, Maxwell's equation:

$$\nabla \times \nabla \times \vec{A} = \frac{4\pi}{c}[\delta(z)\vec{J} + \vec{j}_a], \tag{19}$$

while, within the 2D superconducting film, $\vec{J}$ obeys London's equation [23]:

$$\vec{J} = \frac{c}{2\pi\Lambda}(\vec{\Phi} - \vec{A}), \tag{20}$$

where $\Lambda = 2\lambda^2/d$ is the effective penetration depth for 2D superconductors. The 2D 'fluxoid' field $\vec{\Phi}(\vec{r}, t)$ describes vortex excitations at $\vec{r} = \vec{r}_j(t)$ and satisfies the equation [23]:

$$\nabla \times \vec{\Phi} = \phi_0 \sum_j \delta(\vec{r} - \vec{r}_j). \tag{21}$$

By means of the Fourier-transform method first applied by Pearl [23] to a similar problem, equations (19) and (20) can be solved for the $\vec{q}$-Fourier component, $\underset{\sim}{\delta\vec{A}}(\vec{q}, z, t)$, of $\delta\vec{A}(\vec{r}, z, t)$ giving:

$$\underset{\sim}{\delta\vec{A}}(\vec{q}, z, t) = [\underset{\sim}{\vec{\Phi}}(\vec{q}, t) - \underset{\sim}{\vec{A}}_a(\vec{q}, 0, t)]\frac{e^{-q|z|}}{1 + q\Lambda}, \tag{22}$$

where $\underset{\sim}{\vec{A}}_a(\vec{q}, 0, t)$ is related to $\underset{\sim}{\vec{j}}_a(\vec{q}, q_z, t)$, the 3D Fourier transform of $\vec{j}_a(\vec{r}, z, t)$, by [23]:

$$\underset{\sim}{\vec{A}}_a(\vec{q}, 0, t) = \frac{2\pi}{cq}\underset{\sim}{\vec{j}}_a(\vec{q}, q_z = -iq, t). \tag{23}$$

The Fourier component of the Meissner sheet current density is easily obtained from equations (19) and (20) by setting $\vec{\Phi} = 0$ [23]:

$$\underset{\sim}{\vec{J}}_M(\vec{q}, t) = -\frac{\underset{\sim}{\vec{j}}_a(\vec{q}, q_z = -iq, t)}{1 + q\Lambda}. \tag{24}$$

As it clearly results from equation (21), which contains the vortex positions $\{\vec{r}_j(t)\}$, the vortex dynamics enters the expresion (22) for $\underset{\sim}{\delta\vec{A}}(\vec{q}, z, t)$ through $\underset{\sim}{\vec{\Phi}}(\vec{q}, t)$ which is easily deduced from equation (21) if one notices that, as required by current continuity, $\nabla \cdot \vec{\Phi} = 0$:

$$\underset{\sim}{\vec{\Phi}}(\vec{q}, t) = i\phi_0 \frac{(\hat{q} \times \hat{z})}{q} \sum_j e^{-i\vec{q}\cdot\vec{r}_j(t)}. \tag{25}$$

Writing $\vec{r}_j(t)$ in the form $\vec{r}_j(t) = \vec{r}_{je} + \vec{s}(\vec{r}_{je}, t)$, equation (25) can now be linearized in the small oscillating displacement $\vec{s}(\vec{r}_{je}, t)$ of the vortex j about its static equilibrium position $\vec{r}_{je}$. Then, assuming again an $e^{i\omega t}$-time dependence for all fields and combining equations (22)–(25), the $(\vec{q}, \omega)$-Fourier component, $\underset{\sim}{\delta\vec{E}}_\omega(\vec{q}, z) = -(i\omega/c)\,\underset{\sim}{\delta\vec{A}}_\omega(\vec{q}, z)$, of the electric field $\delta\vec{E}(\vec{r}, z, t)$ generated by $\vec{J}(\vec{r}, t)$ can be written in the form:

$$\underset{\sim}{\delta E}_{\omega\alpha}(\vec{q}, z) = -\frac{e^{-q|z|}}{1+q\Lambda}\left[\sum_{q',\beta} R_{\omega\alpha\beta}(\vec{q}', \vec{q})\,\underset{\sim}{J}_{M\omega\beta}(\vec{q}') + i\omega L_K \frac{1+q\Lambda}{q\Lambda}\,\underset{\sim}{J}_{M\omega\alpha}(\vec{q})\right], \quad (26)$$

where $L_K = 2\pi\Lambda/c^2$ is the sheet kinetic inductance. The first term on the right-hand side of equation (26) is the contribution to $\underset{\sim}{\delta\vec{E}}_\omega(\vec{q}, z)$ due to the oscillating motion of the vertices. Thus, $R_{\omega\alpha\beta}(\vec{q}', \vec{q})$ is the 'vortex response function' in which we are primarily interested here. Using equation (5) for $\vec{s}_\omega(\vec{r}_{je})$ in the linearized equation for $\underset{\sim}{\vec{\Phi}}_\omega(\vec{q})$, it is readily shown that:

$$R_{\omega\alpha\beta}(\vec{q}', \vec{q}) = (\hat{q}\times\hat{z})_\alpha \frac{R_\square}{N^2}\sum_j e^{-i\vec{q}\cdot\vec{r}_{je}} \sum_{\mathbf{K}} \frac{i\omega\tau(\vec{K})}{1+i\omega\tau(\vec{K})}[\hat{q}\cdot\vec{\Phi}_{\mathbf{K}}(\vec{r}_{je})]$$
$$\times \sum_l e^{i\vec{q}'\cdot\vec{r}_{le}}[\hat{z}\times\vec{\Phi}^*_{\mathbf{K}}(\vec{r}_{le})]_\beta, \quad (27)$$

where $\tau(\vec{K}) = \eta/E(\vec{K})$ is the relaxation time for the mode of wave vector $\vec{K}$ and N the total number of vortices in the superconducting film. The last term in equation (26) is the purely inductive contribution to $\underset{\sim}{\delta\vec{E}}_\omega(\vec{q}, z)$ associated with the Meissner response of the superconducting film to the rf-excitation. For weak magnetic fields this term is independent of B and, consequently, it does not contribute to the $\partial V/\partial B$-signal measured in our experiments. Notice that, using equation (24), $\underset{\sim}{\delta\vec{E}}_\omega(\vec{q}, z)$ can alternatively be expressed in terms of $\underset{\sim}{\vec{j}}_{a\omega}(\vec{q}, q_z = -iq)$ rather than of $\underset{\sim}{\vec{J}}_{M\omega}(\vec{q})$.

In the following we shall discuss the rf-response of the 2D vortex crystal in the different phases it can assume on the periodic substrate.

A. *The commensurate* (C) *phase*

With the vortex crystal in a C-phase, the eigenvectors $\vec{\Phi}_{\mathbf{K}}(\vec{r}_{je})$ appearing in equation (27) are given by equation (7) and, moreover, the $\{\vec{r}_{je}\}$ form a set of lattice vectors. Then, from equation (27) it immediately follows:

$$R_{\omega\alpha\beta}(\vec{q}', \vec{q}) = R_\square(\hat{q}\times\hat{z})_\alpha \sum_{\mathbf{K}} \frac{i\omega\tau(\vec{K})}{1+i\omega\tau(\vec{K})}$$
$$\times[\hat{q}\cdot\hat{e}_t(\vec{K})][\hat{z}\times\hat{e}_t(\vec{K})]_\beta \Delta(\vec{K}-\vec{q})\,\Delta(\vec{K}-\vec{q}'), \quad (28)$$

where the Peierls symbol $\Delta(\vec{p})$ is such that $\Delta(\vec{p}) = 1$ if $\vec{p} = \vec{g}_{mn}$ and vanishes otherwise. From equation (28) it is readily seen that only U-processes contribute to the sum over $\vec{K}$, the scalar product in equation (28) vanishing for $\vec{K} = \vec{q}$. Their contribution to the rf-voltage V, however, is vanishingly small, since, as it follows by considering the exponential factor e^{-qh_R} (where $h_R \gg a$) resulting from the integration of equation (26) over the turns of the receive coil R, the relevant $\vec{q}$-vectors of our experiments are such that $qh_R < 1$ and are therefore confined to the first Brillouin zone ($qa \ll 1$). Thus, we can conclude that $\partial V/\partial B \simeq 0$ for an infinite ideal vortex crystal in a C-phase.

B. *The incommensurate* (I) *phase – Size effects*

In an I-phase the eigenvectors $\vec{\Phi}_{\mathbf{K}}$ are given by equation (9). Moreover, $\vec{r}_{je}$ can be written in the form $\vec{r}_{je} = \vec{r}_{j0} + \vec{w}_{je}$, where $\vec{r}_{j0}$ is a lattice vector of the undistorted triangular vortex lattice and $\vec{w}_{je}$ is the periodic [period $P(\delta)$] transverse ($\vec{w}_{je} \cdot \vec{K} = 0$) deformation field associated with the static 1D soliton superlattice. If one assumes that $\vec{w}_{je}$ varies slowly with the position of the vortex j, the sums over j and l in equation (27) can be replaced by integrals over a smooth density of lattice points. Then, a straightforward calculation leads to the following expression for the vortex response function:

$$R_{\omega\alpha\beta}(\vec{q}', \vec{q}) = R_{\square}(\hat{q} \times \hat{z})_{\alpha} \sum_{\mathbf{K}} \frac{i\omega\tau(\vec{K})}{1 + i\omega\tau(\vec{K})} [\hat{q} \cdot \hat{e}_t(\vec{K})][\hat{z} \times \hat{e}_t(\vec{K})]_{\beta} \times \sum_{\vec{G},\vec{G}'} \vec{\Psi}_{\mathbf{K}}(\vec{G}) \vec{\Psi}^{*}_{\mathbf{K}}(\vec{G}') \, \delta_{\mathbf{K},\mathbf{q}-\mathbf{G}} \, \delta_{\mathbf{K},\mathbf{q}'-\mathbf{G}'}, \tag{29}$$

where $\vec{\Psi}_{\mathbf{K}}(\vec{G})$ is the $\vec{G}$-Fourier component of the 'wave function' $\vec{\Psi}_{\mathbf{K}}(u)$, of period P, appearing in equation (9). In our granular Al-films the correlation length R_c sets an upper limit to P ($P \leqslant L \simeq R_c$) which is therefore expected to be much less than h_R ($P \ll h_R$). Since, as shown in the previous subsection, only long-wavelength Fourier components, such that $qh_R < 1$, are important in our experiments, it follows that the relevant $\vec{q}$-vectors are confined within the first Brillouin zone of the 1D soliton superlattice ($qP \ll 1$). Then, by considering the sum over $\vec{K}$ in equation (29), it is readily seen that only U-processes in the reciprocal soliton lattice, such that $\vec{K} = \vec{q} - \vec{G}$ and $\vec{K} = \vec{q}' - \vec{G}'$, contribute to $R_{\omega\alpha\beta}(\vec{q}', \vec{q})$. Furthermore, since $qP \ll 1$ and, consequently, $q \ll G$ and $q' \ll G'$ for the U-processes of interest here, we can set $\vec{K} = \vec{G}$ in equation (29), an approximation which, in turn, implies $\vec{q} \simeq \vec{q}'$. Substituting the resulting diagonal vortex response function into equation (26) and integrating $\overline{\delta\vec{E}}_{\omega}(\vec{r}, z)$ over the turns of the receive coil R, the rf-voltage V can be written in the form:

$$V_{\omega} = C(T) Z'(\omega, B, T) I_{a\omega}. \tag{30}$$

In this expression the 'impedance' $Z'(\omega, B, T)$ contains the vortex dynamics and is given by:

$$Z'(\omega, B, T) = R_{\square} \sum_{\vec{G}}{}' \langle \Phi_{\mathbf{G}}(u) \rangle^2 \frac{i\omega\tau(\vec{G})}{1 + i\omega\tau(\vec{G})}. \tag{31}$$

where the sum is over all $\vec{G}$ excluding the $\vec{G} = 0$-mode and the average of $\Phi_{\mathbf{G}}(u)$, which is given by equation (16) for a piece-wise parabolic potential $U(\phi_e)$, is taken over one period P of the soliton lattice. It is easily verified that only those solutions, $k_{\mathbf{G}}$, of equation (15) which correspond to an even standing wave, i.e. to points like A in Fig. 6, lead to a non-vanishing average of $\Phi_{\mathbf{G}}(u)$.

The temperature dependent factor $C(T)$ describes the geometry of the drive and receive coils as well as their orientation with respect to $\vec{q}_0$. If one assumes a unidirectional Meissner sheet supercurrent density of the form $\vec{J}_{M\omega}(\vec{q}) = \hat{D}\chi_D(\vec{q}) I_{a\omega}$ [see Section II, Fig. 1 and equation (24)], $C(T)$ can be written as:

$$C(T) = \int d^2q \frac{e^{-qh_R}}{1 + q\Lambda(T)} \chi_D(\vec{q}) \chi_R(\vec{q}) \Gamma(\hat{q}), \tag{32}$$

where $\chi_D(\vec{q})$ and $\chi_R(\vec{q})$ are 'circuit functions' depending on the geometrical properties of the drive and receive coils respectively. The factor $\Gamma(\hat{q})$ is given by $\Gamma(\hat{q}) = (\hat{q} \cdot \hat{e}_t)[\hat{e}_t \cdot (\hat{z} \times \hat{D})][\hat{q} \cdot (\hat{z} \times \hat{R})]$ and therefore describes the angular dependence of the vortex response [$\hat{e}_t$ is perpendicular to the direction u of the 1D soliton lattice (Fig. 1)]. It should be noticed that current continuity requires $\vec{q} \cdot \vec{J}_{M\omega}(\vec{q}) = 0$, a condition implying that $\hat{q} \cdot \hat{D} = 0$ for the nearly unidirectional $\vec{J}_M$ of our experiments.

Before proceeding to a qualitative analysis of the experimental data of Section II in terms of the theoretical model studied in Sections III and IV, we recall that the results of this subsection can be applied to a sample of finite size L provided one replaces P by L when the vortex lattice in in a C-phase with boundary solitons (Fig. 7). As shown in Section III(C), in granular films L is of the order of R_c, the Larkin-Ovchinnikov correlation length [21].

C. *Comparisons with experiment and discussion*

Let us first discuss the magnetic field and temperature dependence of the structures observed in $\partial V/\partial B$ about B_{10}. In this connection we notice that $q\Lambda(T) \ll 1$ for the temperatures and q-values ($qh_R < 1$) of interest here and, consequently, $C(T)$ [equation (32)] becomes independent of temperature. {$C(T)$ depends on T only in a narrow temperature range close to T_c, where $\Lambda(T)$ diverges and, as a consequence, $C(T)$ tends to zero as $[1-(T/T_c)]$}. Then, as shown by equation (30), the dependence of the rf-signals on B and T can be simply deduced from numerical calculations of the vortex impedance Z' [equation (31)]. Three parameters enter such calculations: the 'sample size' L, the ratio $\Delta/\mu = (\pi\varepsilon/2q_0)^2$ [24] and the relaxation time $\tau_\Delta = \eta/q_0^2\Delta$ associated with overdamped vortex motion in the periodic pinning potential. Thermal fluctuations of the vortices are roughly taken into account by replacing Δ with $\Delta_R(T)$, the 'renormalized' strength of the pinning potential calculated in Ref. 7 using a self-consistent harmonic approximation. Theoretical field derivatives of the normalized impedance $z' = Z'/R_\square$, as deduced from equation (31) using equation (16) for $\Phi_{\mathbf{G}}(u)$, equation (15) for $k_{\mathbf{G}}$, equation (11) for $P[\delta(B)]$ and equation (14) for $\tau(\vec{G}) = \eta/E(\vec{G})$, are shown in Fig. 8 for a typical domain size ($L = R_c = 30\lambda_0$) and for values of Δ_R/μ and $\omega\tau_{\Delta R}$ corresponding to three different temperatures. Comparison with the data in Fig. 2 shows good qualitative agreement for the field dependence as well as for the relative magnitude of the real and imaginary parts of the $\partial V/\partial B$-signal. As observed experimentally, the model correctly predicts, for rising temperatures, a gradual decrease of the structures around B_{10} followed by a rapid degradation when T approaches the 'locking-unlocking' temperature T_{LU} [7], above which the vortex lattice no longer feels the periodic pinning structure [$\Delta_R(T_{LU}) = 0$]. At very low temperatures ($T \to 0$), Δ_R/μ and $\omega\tau_{\Delta R}$ become independent of T and, as a consequence, the structures in $\partial V/\partial B$ reach their maximum amplitude. This is in striking contrast with the complete absence of structures in the rf-data taken at temperatures below $\sim$1.7 K. This behaviour might be due to the growing (relative) importance of random pinning effects with decreasing temperatures. Further work is needed, however, in order to assess the validity of this conjecture.

To discuss the low-temperature angular dependence of the rf-signals (Fig. 4), we must consider the $\Gamma(\hat{q})$-factor in equation (32). In this connection, we first

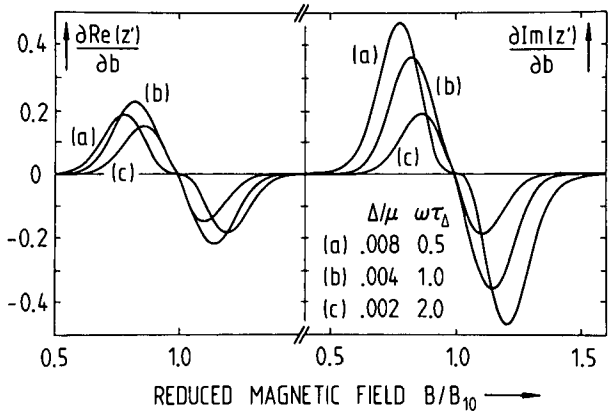

Figure 8
Theoretical field derivatives of the normalized vortex impedance $z' = Z'/R_{\square}$ calculated from equation (31) for three different temperatures. b is the reduced magnetic field B/B_{10}.

notice that all the experimental data presented in this paper were obtained with a drive-receive coil configuration such that $\hat{D}//\hat{R}$ (Fig. 1). As discussed in Section III(C), in granular Al-films the vortex lattice is expected to break up into a large number of uncorrelated domains. For the sake of illustration, we first consider the rather unlikely situation in which the soliton lattice is supposed to have the same orientation, say at +45° with respect to $\vec{q}_0$ (the u-direction in Fig. 1), in all domains. In this case $\Gamma(\hat{q})$ has the same value for both the (x, x)- and the (y, y)-configurations: $\Gamma_{xx} = \Gamma_{yy} = 1/2$. For the $(x+y, x+y)$-configuration we distinguish two cases: (i) $\hat{D}$ (and $\hat{R}$) parallel to the soliton lattice, for which $\Gamma_{x+y,x+y} = 1$ and (ii) $\hat{D}$ (and $\hat{R}$) perpendicular to the soliton lattice, for which $\Gamma_{x+y,x+y} = 0$. This strongly anisotropic behaviour of the low-temperature dynamic vortex response was not observed in our experiments. On the other hand, if one assumes that the vortex crystal breaks up into uncorrelated domains in which the orientation of the solitons randomly changes from +45° to −45° with respect to $\vec{q}_0$, a simple averaging procedure, which assumes an equal number of domains for the two possible orientations, leads to $\langle\Gamma(\hat{q})\rangle = \Gamma_{xx} = \Gamma_{yy} = \Gamma_{x+y,x+y} = 1/2$. This reasonably agrees with the nearly isotropic rf-response observed at low temperatures (Fig. 4), a result providing convincing evidence for a multidomain structure with solitons randomly oriented at ±45° with respect to the thickness modulation.

At high temperatures, where a new strongly anisotropic signal shows up in the rf-data (Figs. 3 and 5), our model fails in describing the dynamic vortex response. This might be due to the formation of liquid-like domains in a temperature range which is above the 2D melting temperature [9–11]. Calculations of the dynamic response in such a régime will be done in the near future.

Acknowledgements

We would like to thank J. R. Clem and V. L. Pokrovsky for many stimulating discussions. This work has been supported by the Swiss National Science Foundation.

REFERENCES

[1] P. BAK, Prog. Phys. *45*, 587 (1982).
[2] O. DALDINI, P. MARTINOLI, J. L. OLSEN and G. BERNER, Phys. Rev. Lett. *32*, 218 (1974).
[3] P. MARTINOLI, O. DALDINI, CH. LEEMANN and E. STOCKER, Solid State Commun. *17*, 205 (1975).
[4] P. MARTINOLI, O. DALDINI, CH. LEEMANN and B. VAN DEN BRANDT, Phys. Rev. Lett. *36*, 382 (1976).
[5] P. MARTINOLI, Phys. Rev. B *17*, 1175 (1978).
[6] P. MARTINOLI, H. BECK, M. NSABIMANA and G. A. RACINE, Physica *107B*, 455 (1981).
[7] P. MARTINOLI, M. NSABIMANA, C. A. RACINE, H. BECK and J. R. Clem. Helv. Phys. Acta *55*, 655 (1982).
[8] V. L. POKROVSKY and A. L. TALAPOV, Phys. Rev. Lett. *42*, 65 (1979); Sov. Phys. JETP *51*, 134 (1980).
[9] J. M. KOSTERLITZ and D. J. THOULESS, J. Phys. C *6*, 1181 (1973).
[10] B. A. HUBERMAN and S. DONIACH, Phys. Rev. Lett. *43*, 950 (1979).
[11] D. R. NELSON and B. I. HALPERIN, Phys. Rev. B *19*, 2457 (1979).
[12] A. T. FIORY, Phys. Rev. B *8*, 5039 (1973).
[13] A. T. FIORY and A. F. HEBARD, AIP Conf. Proc. *58*, 293 (1980).
[14] J. R. CLEM, private communication.
[15] L. LANDAU and E. LIFSHITZ, *Theory of elasticity* (Pergamon Press, London, 1970), Ch. III.
[16] J. BARDEEN and M. J. STEPHEN, Phys. Rev. *140A*, 1197 (1965).
[17] S. E. BURKOV and V. L. POKROVSKY, J. Low Temp. *44*, 423 (1981).
[18] F. PATTHEY, M. S.-THESIS (Université de Neuchâtel, 1984), unpublished.
[19] S. FLÜGGE, *Rechenmethoden der Quantentheorie* (Springer-Verlag, Berlin, 1965), p. 59.
[20] P. A. LEE, T. M. RICE and P. W. ANDERSON, Solid State Commun. *14*, 703 (1974).
[21] A. I. LARKIN and YU. N. OVCHINNIKOV, J. Low Temp. Phys. *34*, 409 (1979).
[22] P. H. KES and C. C. TSUEI, Phys. Rev. B *28*, 5126 (1982).
[23] J. PEARL, PhD-Thesis (Polytechnic Institute of Brooklyn, New York, 1965), unpublished.
[24] As shown in Ref. 7, Δ/μ is of the order of $4(\Delta d/d)$.

Proc. 18th Int. Conf. on Low Temperature Physics, Kyoto, 1987
Japanese Journal of Applied Physics, Vol. 26 (1987) Supplement 26-3

Shear Modulus Softening of a Lattice of Superconducting Vortices

X.-M. TANG, G.-A. RACINE, Ch. LEEMANN, and P. MARTINOLI

Institut de Physique, Université de Neuchâtel, CH-2000 Neuchâtel, Switzerland

The critical currents of superconducting films, in which the vortex lattice is exposed to the pinning field created by a periodic thichness modulation, show an unusual non-monotonic temperature dependence near the superconducting transition. This anomalous feature, which is observed when the flux lattice is commensurate with the periodic film structure, is consistent with a softening of the shear modulus of the vortex lattice due to anharmonic "phonon-phonon" interactions.

The lattice of quantized vortices in thin superconducting films can be thought of as an incompressible two-dimensional (2D) crystal whose long-wavelength properties are determined by a single elastic constant, the shear modulus μ. At non-zero temperatures μ is renormalized by nonlinear lattice vibrations associated with "phonon-phonon" interactions and by thermally activated topological defects forming bound pairs of dislocations with opposite Burgers vectors [1,2]. Vortex lattice melting driven by the unbinding of dislocation-antidislocation pairs is predicted to occur at a temperature T_M determined by the Kosterlitz-Thouless criterion for the existence of topological order in two dimensions [2]. While there is some experimental evidence for a solid-to-fluid transition of the vortex lattice [3], no convincing demonstration of dislocation mediated melting has been produced so far, the study of the critical behaviour close to T_M being complicated by vortex pinning phenomena [3,4]. In this letter we report the observation of an unusual non-monotonic temperature dependence of the critical current, I_c, of superconducting layers in which a well-defined pinning structure is introduced by periodically modulating the film thickness in one direction [5]. This anomalous behaviour, which is observed for vortex densities corresponding to lattice configurations commensurate with the periodic film structure [5,7], is consistent with a softening of the vortex lattice due to anharmonic phonon-phonon interactions occurring well below T_M.

The experiments were performed on a granular Al-film with an average thickness, d, of 3000 Å, a relative thickness modulation, $\Delta d/d$, of ~ 20 % and a modulation period, λ_g, of 1.4 μm. Because of the relatively low normal-state sheet resistance $R_\square$ of the Al-layer ($R_\square$ = 0.7 Ω), the estimated T_M practically coincides with the mean-field transition temperature, T_{co} = 1.66 K, of the film [1]. As a function of magnetic field B, the critical current $I_c(B)$ shows characteristic peaks for $B = B_{mn}$, the field values at which the vortex lattice perfectly matches the periodic pinning structure [5-7]. However, as illustrated in Fig. 1 for the fundamental matching configuration at B_{10} = 9.2 gauss, the magnitude of the critical-current peak shows a remarkable temperature dependence characterized by a minimum-maximum structure in the $I_c(t)$-curve ($t = T/T_{co}$) just below T_{co}. At $t^* \approx 0.945$, the reduced temperature corresponding to the minimum, the critical currents of the modulated layer and of a flat reference film are roughly of the same strength, indicating that the additional pinning mechanism provided by the thickness modulation is strongly reduced at t*. This is further demonstrated by the absence, at the same temperature, of quantum interference steps in the current-voltage characteristic of the modulated film exposed to rf radiation [6] (Fig. 2). Notice, however, that the quantum steps reappear, *sharper* than at lower temperatures, for $t > t^*$ and are well resolved up to temperatures very close to T_{co}. This observation implies a highly correlated motion of the vortices and, therefore, the existence of a solid-like vortex medium in this temperature region. This is consistent with our estimate $T_M \approx T_{co}$. Another feature of the critical-current data is worth mentioning. From the width, $2\Delta B$, of the I_c-peak at B_{10} it is possible to deduce the critical mismatch parameter $\delta_c \approx \Delta B/2B_{10}$ at which the vortex lattice undergoes the transition from the commensurate to the incommensurate phase [7]. The temperature dependence of δ_c is shown in Fig. 3 : $\delta_c(t)$ exhibits a shallow minimum approximately at t*.

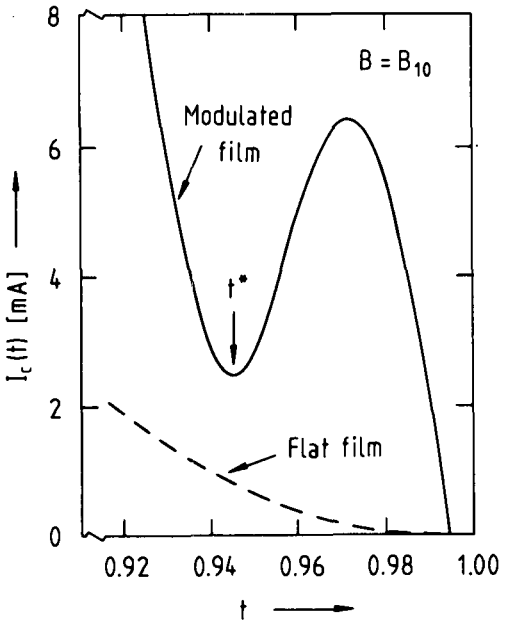

Fig. 1. Anomalous temperature dependence of the critical-current peak at B_{10} of a thickness-modulated film.

A simple model accounts for the essential features of our experiments. We start by writing the expressions for the critical current density at B_{mn}

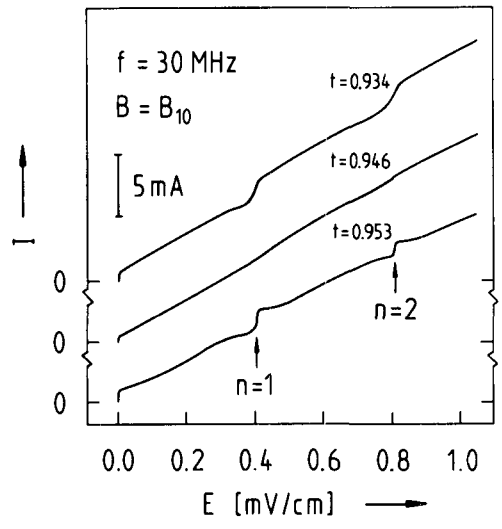

Fig. 2. Current-voltage curves at different reduced temperatures of a thickness-modulated film exposed to rf radiation. Quantum steps at $E_n = nf\lambda_g B_{10}$ disappear for $t \approx t^*$.

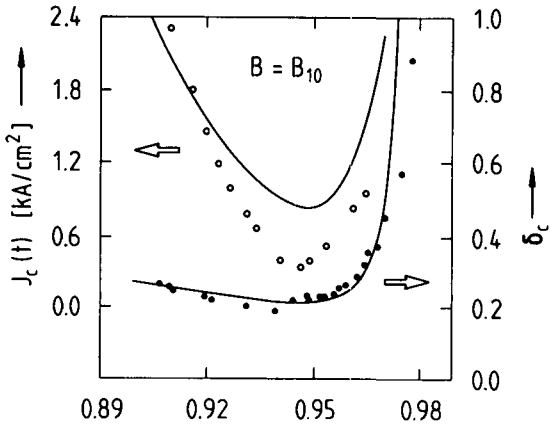

Fig. 3. Critical current density (open circles) and critical mismatch parameter (full circles) as a function of reduced temperature at B_{10}. Solid lines are theoretical predictions based on Eqs. (1)-(4).

$$j_c(T) = (2\pi/\phi_0\lambda_g d)\Delta_R(T) \qquad (1)$$

and for the critical mismatch

$$\delta_c(T) = (2/\pi)\,[\Delta_R(T)/\mu(T)]^{1/2} \qquad (2)$$

derived in Ref. [7]. In Eqs. (1) and (2) $\Delta_R(T)$ is the amplitude of the periodic pinning potential renormalized (R) by thermal fluctuations of the vortices around their equilibrium positions at the bottom of the potential wells. $\Delta_R(T)$ is given by [7] :

$$\Delta_R(T)/\Delta(T) = [\Delta(T)/\mu(T)]^{T/(T_{LU}-T)} \quad , \qquad (3)$$

where $\Delta(T)$ and $\mu(T)$ are, respectively, the bare pinning potential amplitude and the shear modulus and T_{LU} is the locking-unlocking temperature [7], essentially T_{co} in our low-sheet-resistance film. If one neglects the renormalization of $\mu(T)$, the ratio $\Delta(T)/\mu(T)$ is independent of T [7] ($\Delta/\mu \approx 4\Delta d/d$), leading to a monotonic temperature dependence for both $j_c(T)$ and $\delta_c(T)$. Non-linear lattice vibrations and dislocation pairs, however, renormalize the shear modulus at finite temperatures. Since no evidence was found for vortex lattice melting and the temperature region of interest is well below the estimated T_M, we neglect the effect of dislocation pairs. Then, renormalization due to phonon-phonon interactions leads to [1] :

$$\mu_R(T) = \mu(T)\{1-C[4\pi^2 k_B T\Lambda(T)/\phi_o^2]\} \quad , \qquad (4)$$

where $\Lambda(T)$ is the effective thin film penetration depth [7] and C a numerical constant, the only adjustable parameter of the model. If we now assume that the effect of vortex lattice softening on $j_c(T)$ and $\delta_c(T)$ can be simply described by replacing $\mu(T)$ with $\mu_R(T)$ in Eqs. (1)-(3), then we obtain the theoretical curves shown in Fig. 3. The expression of $\mu(T)$ valid at intermediate fields [1,7] has been used in the calculations. The agreement is excellent for $\delta_c(T)$, while it is only qualitative for $j_c(T)$. This is possibly due to the method used to obtain the j_c-data, a procedure involving the subtraction of the two $I_c(t)$-curves shown in Fig. 1.

The physical picture emerging from our analysis is quite simple. Below t*, the main effect of thermal fluctuations is to renormalize Δ, causing j_c and δ_c to decrease with rising temperatures. Vortex lattice softening, on the other hand, is the dominant phenomenon above t*, an effect making vortex pinning more effective and, consequently, causing j_c and δ_c to rise with temperature.

This work was supported by the Swiss National Science Foundation.

REFERENCES

1) D.S. Fisher: Phys. Rev. B22 (1980) 1190.
2) D.R. Nelson and B.I. Halperin: Phys. Rev. B19 (1979) 2457.
3) A.T. Fiory and A.F. Hebard: Phys. Rev. B25 (1982) 2073.
4) P.H. Kes and C.C. Tsuei: Phys. Rev. B28 (1983) 5126.
5) O. Daldini, P. Martinoli, J.L. Olsen and G. Berner: Phys. Rev. Lett. 32 (1974) 218.
6) P. Martinoli: Phys. Rev. B17 (1978) 1175.
7) P. Martinoli, M. Nsabimana, G.A. Racine and H. Beck: Helv. Phys. Acta 55 (1982) 655.

Inductive conductance measurements in two-dimensional superconducting systems

B. Jeanneret, J. L. Gavilano, G. A. Racine, Ch. Leemann, and P. Martinoli
Institut de Physique, Université de Neuchâtel, CH-2000 Neuchâtel, Switzerland

(Received 25 August 1989; accepted for publication 29 September 1989)

A two-coil mutual-inductance technique for measuring the complex ac response of a two-dimensional (2-D) superconductor to a weak ac magnetic field is described. Analytical and numerical methods are presented which allow extraction of the complex ac conductance of the superconductor from the signal voltage induced in the detection coil by the screening currents flowing in the sample. The method is illustrated by measurements of the ac conductance of a square network of aluminum wires from which the penetration depths of both the network and (granular) aluminum are deduced. It is shown that the method provides a powerful tool to observe characteristic features associated with critical phenomena in 2-D superconducting systems.

The response of a superconductor to time-dependent electromagnetic fields can be described in terms of the complex ac conductivity of the system. Conductivity measurements probe the dynamics of the accelerated superfluid and of low-energy excitations from the superconducting ground state such as quasiparticles and vortices. A particularly attractive aspect of experiments focusing on the ac conductivity is the possibility to perform accurate measurements of a fundamental parameter of superconductivity, the magnetic penetration depth, and to explore in detail the nature of various dissipative processes.

A two-coil mutual-inductance technique for measuring the low-frequency complex sheet conductance (rather than the ac conductivity) of two-dimensional (2-D) superconductors was first devised by Fiory and Hebard,[1] who used it to study thin films of aluminum/aluminum-oxide[2] and indium/indium-oxide composites[3] and, recently epitaxial YBaCuO layers.[4] In recent work, we used a modified version of Fiory–Hebard's method to investigate magnetic screening and dissipation in connection with critical phenomena in 2-D arrays of proximity effect Josephson junctions,[5] in 2-D wire networks[6] and in granular high T_c films.[7] In consideration of the current widespread interest in thin films of the novel superconducting oxides, in this letter we give a thorough account of our drive-receive coil technique which has been only marginally described in previous work. Relying on accurate control of the two-coil geometry to model ac currents and fields, we derive an *analytical* expression relating the signal voltage δV at the receiver to the ac sheet conductance G of the sample. This distinctive aspect of our method favors the use of a very simple yet powerful numerical inversion procedure[4] to extract G from δV, thereby providing detailed insight into the physics of 2-D superconductors.

At the heart of the ac conductance measuring system, shown in Fig. 1, there are a drive coil of radius $R_D = 2.05$ mm and a pair of astatically wound receive coils of radius $R_R = 1.2$ mm coaxially mounted within the excitation coil. Mechanical stability is achieved by embedding the coil assembly in stycast. The drive coil has $N_D = 23$ turns equally spaced by $\delta h_D = 0.2$ mm, and is placed at a distance h_D of 0.3 mm from the sample. The two mutually compensating sections of the detection coil have $N_R = 15$ turns each of 20-μm-diam wire, the uniform spacing δh_R between the turns being the only adjustable parameter used in the calibration procedure outlined below (δh_R is of the order of 30 μm). The gradiometer configuration of the receiver favors sensitivity to currents flowing in the film with respect to those circulating in the drive coil and helps to suppress external flux noise. To achieve maximum sensitivity, the distance h_R of the lower detection coil to the sample is kept as small as possible (h_R is at least an order of magnitude smaller than h_D). The in-phase and quadrature components of the voltage δV at the receive coil due to the screening currents flowing in the superconducting sample in response to an ac current of amplitude I_D and angular frequency ω in the drive coil are detected by conventional lock-in techniques or by an ac mutual-inductance bridge incorporating a superconducting quantum interference device (SQUID) detector. To illustrate our method we present conductance measurements performed on a network of aluminum wires[6] of width $w = 1.4\,\mu$m forming a square lattice with 10^6 nodes connected by strips of length $a = 8\,\mu$m and normal-state resistance

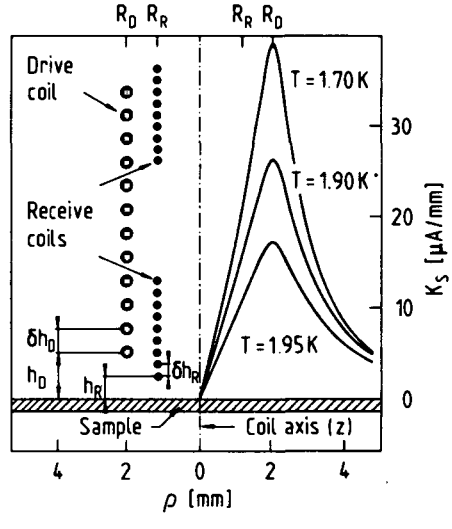

FIG. 1. Left side: geometry of the drive-receive coil system. Right side: radial sheet current density distribution in a superconducting network of Al wires as computed from Eq. (4) for three different temperatures ($I_D = 15$ μA).

 0003-6951/89/482336-03$01.00

$R_s = 95\ \Omega$. The sample was patterned from a 400-Å-thick granular Al film using standard photolithography and wet etching.

To study the response of the superconducting system to the ac magnetic field created by the drive coil, we first derive an expression for the sheet current density $\mathbf{K}_s$ in the sample, which is assumed to be homogeneous and isotropic over the characteristic length scales selected by the coils. We use cylindrical coordinates defined by $\mathbf{r} = (\rho,\phi,z)$ and locate the 2-D sample in the $z = 0$ plane, the axis of the coil arrangement coinciding with the z axis. Then, in the gauge $\nabla\cdot\mathbf{A} = 0$, Ampère's law for the total vector potential $\mathbf{A}(\mathbf{r})$ can be written as

$$-\nabla^2\mathbf{A}(\rho,z) = \mu_0[\mathbf{K}_s(\rho)\delta(z) + \mathbf{j}_D(\rho,z)], \tag{1}$$

where $\mathbf{j}_D(\rho,z)$ is the current density distribution generated by the drive coil

$$\mathbf{j}_D(\rho,z) = I_D\delta(\rho - R_D)\sum_{n=0}^{N_D-1}\delta(z - h_D - n\delta h_D)\hat{\varphi}. \tag{2}$$

Because of the high degree of precision achieved in controlling the geometrical parameters of the coils in the fabrication process, Eq. (2) is believed to provide a very accurate description of the driving current density. Neglecting normal current contributions and taking an $\exp(i\omega t)$-time dependence for all fields, we define G by $\mathbf{K}_s(\rho) = G(\omega)\mathbf{E}(\rho,z=0) = -i\omega G(\omega)\mathbf{A}(\rho,z=0)$. In writing this local relation, we implicitly assume that finite $\mathbf{q}$ corrections to G can be ignored for the wave vectors selected by our coil configurtion. By Fourier transforming and solving Eq. (1) for $\mathbf{K}_s$ using the formalism developed by Pearl,[8] we obtain

$$\mathbf{K}_s(q_t) = -\frac{\mathbf{j}_D(q_t,q_z = -iq_t)}{1 + (2/i\omega G)q_t}, \tag{3}$$

where q_t and q_z are, respectively, the in-plane and axial components of $\mathbf{q}$. Then, using the driving current distribution of Eq. (2), a straightforward transformation of Eq. (3) back to real space leads to the following expression for $\mathbf{K}_s(\rho)$:

$$\mathbf{K}_s(\rho) = I_D R_D\int_0^\infty dq_t\,\frac{q_t e^{-q_t h_D}}{1 + (2/\mu_0)(1/i\omega G)q_t} \times J_1(q_t R_D)J_1(q_t\rho)\frac{1 - e^{-q_t N_D\delta h_D}}{1 - e^{-q_t\delta h_D}}\hat{\varphi}, \tag{4}$$

where $J_1(x)$ is the first-order Bessel function. As an example, in Fig. 1 we show the screening current distribution resulting from Eq. (4) for the superconducting network described above. At the three temperatures indicated in the figure, this sample behaves as a pure inductor with $G = (i\omega L_k)^{-1}$, where $L_k(T)$ is the network kinetic inductance[6] discussed in detail in the last section of the paper. As expected, $\mathbf{K}_s(\rho)$ has a maximum at $\rho = R_D$, whose strength reflects the linear variation of $L_k^{-1}(T)$ in the temperature range of interest, near the mean-field critical temperature of the network ($T_{c0} = 1.995$ K).

Having found an expression for $\mathbf{K}_s$, we proceed to compute δV by observing that the Fourier transform of the electric field $\delta\mathbf{E}(\rho,z)$ generated by the screening currents flowing in the sample is given by $\delta\mathbf{E}(q_t, q_z) = -i\omega\mu_0\mathbf{K}_s(q_t)/(q_t^2 + q_z^2)$, as follows by inspection of Eq. (1). By performing the line integral of $\delta\mathbf{E}(\rho,z)$ over the N_R equally spaced turns of the lower detection coil (contributions to δV from the upper section of the receiver, being exponentially cut off, can be neglected), we find that δV can be written as

$$\delta V = i\omega I_D\int_0^\infty dx\,\frac{M(x)}{1 + (2/\mu_0 h)(1/i\omega G)x}, \tag{5}$$

where $x = q_t h$, with $h = h_D + h_R$. In this relation, which is the central result of this letter, $M(x)$ is a mutual-inductance distribution comprising the geometry of the measuring system and is given by

$$M(x) = \pi\mu_0 h\alpha\beta J_1(\alpha x)J_1(\beta x)e^{-x}\frac{(1 - e^{-N_D\gamma x})}{(1 - e^{-\gamma x})} \times\frac{(1 - e^{-N_R\delta x})}{(1 - e^{-\delta x})}, \tag{6}$$

where α,β,γ, and δ are, respectively, $R_D, R_R, \delta h_D$, and δh_R expressed in units of h. As illustrated in Fig. 2, for $h = 0.3$ mm, $M(x)$ is strongly peaked at $x \approx 0.2$, a value showing that the relevant Fourier components selected by our coil arrangement have wavelengths of the order of 10 mm. Figure 2 also clearly demonstrates that larger values of h would lead to an appreciable loss of signal.

In the following we describe how the ac conductance of our wire network can be extracted from the response of the sample at 70 kHz, shown as a function of temperature in the upper part of Fig. 3, by applying the numerical inversion procedure of Ref. 4 to Eq. (5). To remove most of the dependence on geometrical parameters, G and δV are conveniently expressed in terms of two complex dimensionless variables, $g \equiv |g|\exp(i\theta_g)$ and $u \equiv |u|\exp(i\theta_u)$, defined by $g = 2/i\omega\mu_0 hG$ and $u = (V_{SS}/\delta V) - 1$, where V_{SS} is the (purely inductive) signal generated by a sample in the strong screening limit ($1/G \to 0$). We determine V_{SS} by measuring the voltage jump at T_{c0} induced by a suitably selected superconducting film showing no observable variations of $\mathrm{Im}[\delta V(T)]$ below T_{c0} ($g \ll 1$) and no detectable evidence of

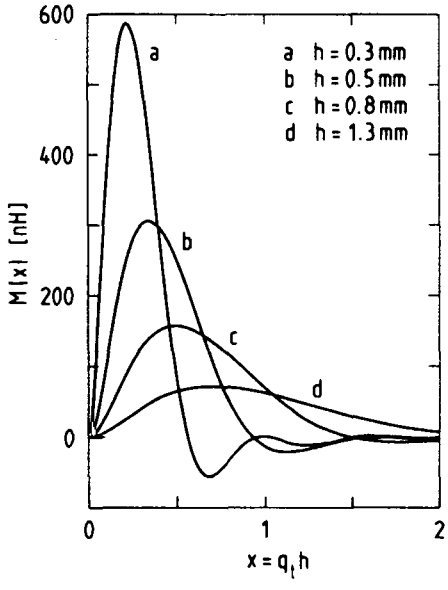

FIG. 2. Geometrical mutual inductance distribution in 2-D q space of the two-coil system shown in Fig. 1 as given by Eq. (6). $h = h_D + h_R$.

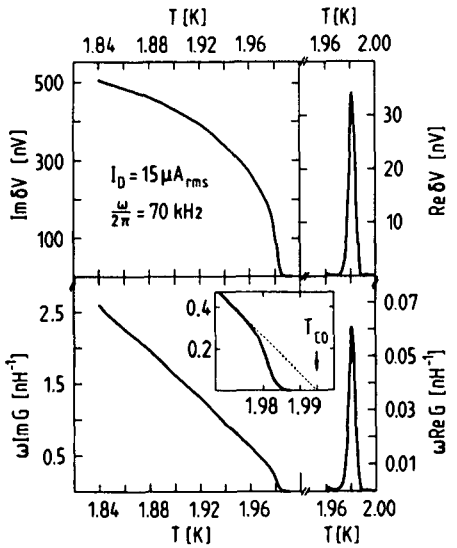

FIG. 3. Upper part: in-phase and quadrature voltage signals vs temperature induced by a superconducting network of Al wires. Lower part: temperature dependence of the complex ac conductance of the network extracted from $\delta V(T)$ by inverting Eq. (5). Inset shows expanded view of the critical region. Dashed straight line is the extrapolated mean field behavior.

eddy currents in the normal state ($g \gg 1$). The measuring system is then calibrated by fitting δ to V_{SS} using Eq. (5). Relying on Eqs. (5) and (6) and on a simple interpolation scheme, two tables, one for θ_u and the other one for the ratio $s = |g|/|u|$, are constructed for a range of values of $|u|$ and θ_g. In both tables, a row corresponds to $|u| = \text{const.}$, while a column is specified by $\theta_g = \text{const.}$ By comparing the data $(|u|,\theta_u)$ with the values in the table for θ_u one reads θ_g and hence, from the corresponding position in the second table, one deduces s, and finally $|g| = s|u|$. Using this simple look-up procedure, we obtain the complex network conductance shown as a function of temperature in the lower part of Fig. 3. With the exception of the critical region, marked by dissipation, the network, as anticipated above, is a pure inductor $[\mathrm{Re}(G) = 0]$ characterized by $\omega\,\mathrm{Im}[G(T)] = L_k^{-1}(T)$. The kinetic inductance is related to the effective penetration depth[6] of the network, $\Lambda(T) = 2(a/w)\lambda^2(T)/d$, where $\lambda(T)$ is the bulk penetration depth, by $L_k(T) = (\mu_0/2)\Lambda(T)$. Thus, as predicted by the Bardeen–Cooper–Schrieffer (BCS) theory[9] at temperatures not too far below T_{c0} one expects $L_k^{-1}(T)$ to be proportional to $(T_{c0} - T)$, in agreement with the observed temperature dependence of $\omega\,\mathrm{Im}[G(T)]$ in Fig. 3. By fitting the inverse kinetic-inductance data of Fig. 3 to the theoretical prediction using the BCS dirty-limit formula for $\lambda(T)$,[9] one finds the value of T_{c0} quoted above and $\lambda(0) = 0.66\ \mu$m [corresponding to $\Lambda(0) = 125\ \mu$m], a value which is within 10% of the theoretical estimate based on the London penetration depth (157 Å), the Pippard coherence length (0.95 μm), and the electronic mean free path (6 Å) of the granular Al film.

In the transition region, the conductance data of Fig. 3 reveal features associated with the critical behavior of the network.[6] At a critical temperature T_c of 1.98 K, just below T_{c0}, we observe a marked drop of the superfluid component accompanied by a peak in dissipation reflecting a phase transition driven by the vortex unbinding mechanism predicted by the Kosterlitz–Thouless theory[10] for 2-D systems. In this connection, it is important to notice that, while there is clear evidence for a "superfluid falloff" at T_c in the imaginary part of the conductance data, almost no trace of this feature is visible in the corresponding signal-voltage data, where it is masked by the convolution of G with the geometry of the coil system described by Eq. (5). This clearly demonstrates the effectiveness of the numerical inversion scheme.

In conclusion, we have shown how a combination of analytical and numerical methods applied to a two-coil mutual-inductance technique provides a powerful tool to study magnetic field penetration effects and critical phenomena in 2-D superconducting systems.

It is a pleasure to thank Ph. Lerch, R. Théron, Ph. Flückiger, R. Rentsch, and R. Meyer for their valuable contributions in developing the two-coil technique and J. R. Clem for providing his unpublished work on screening effects in superconducting films. This work was supported by the Swiss National Science Foundation.

[1] A. T. Fiory and A. F. Hebard, AIP Conf. Proc. **58**, 293 (1980).
[2] A. F. Hebard and A. T. Fiory, Phys. Rev. Lett. **44**, 291 (1980).
[3] A. T. Fiory, A. F. Hebard, and W. I. Glaberson, Phys. Rev. B **28**, 5075 (1983).
[4] A. T. Fiory, A. F. Hebard, P. M. Mankiewich, and R. E. Howard, Appl. Phys. Lett. **52**, 2165 (1988); Phys. Rev. Lett. **61**, 1419 (1988).
[5] Ch. Leemann, Ph. Lerch, G. A. Racine, and P. Martinoli, Phys. Rev. Lett. **56**, 1291 (1986).
[6] B. Jeanneret, Ch. Leemann, and P. Martinoli, Jpn. J. Appl. Phys. **26-3**, 1417 (1987); B. Jeanneret, Ph. Flückiger, Ch. Leemann, and P. Martinoli, IEEE Trans. Magn. **MAG-25**, 1428 (1989); B. Jeanneret, Ph. Flückiger, J. L. Gavilano, Ch. Leemann, and P. Martindi, Phys. Rev. B (to be published).
[7] P. K. Srivastava, P. Debély, H. E. Hintermann, Ch. Leemann, J. Weber, O. Caccivio, P. Martinoli, and H. R. Ott, Physica C **153-155**, 1443 (1988).
[8] J. Pearl, Thesis on: Vortex theory of superconductive memories, Polytechnic Institute of Brooklyn, New York, 1965 (unpublished).
[9] M. Tinkham, *Introduction to Superconductivity* (McGraw-Hill, New York, 1975), p. 80.
[10] M. Kosterlitz and D. J. Thouless, J. Phys. C **6**, 1181 (1973).

Liste des publications:

Les numéros imprimés en gras réfèrent aux tirés à part ci-joints.

[1] P. Martinoli, H. Beck, M. Nsabimana, and G.-A. Racine, *Locking-unlocking transition of a two-dimensional lattice of superconducting vortices*, Physica B 107, 455 (1981)

[2] P. Martinoli, M. Nsabimana, G.-A. Racine, and H. Beck, *Locked and unlocked phases of a two-dimensional lattice of superconducting vortices*, Helvetica Physica Acta 55, 655 (1982)

[3] P. Martinoli, M. Nsabimana, G.-A. Racine, and H. Beck, *Search for two-dimensional melting in a lattice of superconducting vortices*, Physica Acta 56, 765 (1983)

[4] P. Martinoli, H. Beck, M. Nsabimana, and G.-A. Racine, *Static and dynamic properties of commensurate and incommensurate phases of a two-dimensional lattice of superconducting vortices*, in NATO ASI; Percolation, Localization, and Superconductivity (Ed. A.M. Goldman and S.A. Wolf: Plenum Publishing Corp.), 371 (1984)

[5] F. Patthey, G.-A. Racine, Ch. Leemann, H. Beck, and P. Martinoli, *Dynamics of commensurate and incommensurate phases of a two-dimensional lattice of superconducting vortices*, Proc. 17th Int. Conf. on Low-Temperature Physics LT-17, Physica B+C 126, 573 (1984)

[6] P. Martinoli, H. Beck, G.-A. Racine, F. Patthey, and Ch. Leemann, *Commensurate and incommensurate vortex phases in a two-dimensional lattice of superconducting vortices*, Lecture Notes in Physics (Springer Verlag, Berlin), 217, 468 (1984)

[7] P. Martinoli, H. Beck, G.-A. Racine, F. Patthey, and Ch. Leemann, *Dynamics of commensurate and incommensurate vortex phases in a two-dimensional superconductor*, Helvetica Physica Acta 58, 427 (1985)

[8] Ch. Leemann, Ph. Lerch, G.-A. Racine, A. Strupler, and P. Martinoli, *Dynamic conductance of a two-dimensional array of Josephson junctions*, IC-Squid '85, Superconducting Quantum Interference Devices and their Applications (Ed. W. de Gruyter, Berlin 1985)

[9] Ch. Leemann, Ph. Lerch, G.-A. Racine, and P. Martinoli, *Vortex dynamics and phase transition in a two-dimensional array of Josephson junctions*, Physical Review Letter 56, 1291 (1986)

[10] X.-M. Tang, G.-A. Racine, Ch. Leemann, and P. Martinoli, *Shear modulus softening of a lattice of superconducting vortices*, Proc. 18th Int. Conf. on Low-Temperature Physics LT-18, Japanesse Journal of Applied Physics 26, 1497 (1987)

[11] B. Jeanneret, J.L. Gavilano, G.-A. Racine, Ch. Leemann, and P. Martinoli, *Inductive conductance measurements in two-dimensional superconducting systems*, Applied Physics Letters 55, 2336, (1989)